Progress in Oceanography 175 (2019) 226–244

Contents lists available at ScienceDirect

Progress in Oceanography

journal homepage: www.elsevier.com/locate/pocean

The impact of climate change on circulation patterns in the Eastern Mediterranean Sea upper layer using Med-ROMS model

Hazem Nagy[a,c,*], Emanuele Di Lorenzo[b], Ahmed El-Gindy[a]

[a] Oceanography Department, Faculty of Science, Alexandria University, Alexandria, Egypt
[b] School of Earth and Atmospheric Sciences, Georgia Institute of Technology, Atlanta, GA, USA
[c] Marine Institute, Oranmore, Galway, Ireland

ARTICLE INFO

Keywords:
Med-ROMS
Eastern Mediterranean
North Ionian Sea
NAO

ABSTRACT

This paper deals with three hindcasting simulations of circulation and sea level elevation, using Med-ROMS (Mediterranean- Regional Ocean Model System, with high horizontal -resolution (8.6 km). Each simulation has started at the end of previous 100-years spin-up and control run. The model surface boundary conditions, from the corrected ERA-40 re-analyses (Pettenuzzo et al., 2010) and three momentum flux ensemble members are based on a surface wind Bayesian Hierarchical Models (BHM) - Mediterranean Forecasting System (MFS-Wind-BHM) described in Berliner and Kim (2007) and Milliff et al. (2011), cover the period January 1958 to December 2001. The results have been validated by an Empirical Orthogonal Function (EOF) analysis of surface sea height anomalies for satellite and Med-ROMS Hindcasts. The correlation coefficients between Med-ROMS (Principal Component) PC1 (Sea Surface Height anomaly) SSHa hindcasts 1, 2, 3 and AVISO satellite are 0.985, 0.97 and 0.98 respectively, all values are significant at 95% confidence limit. We have defined a Bimodal Oscillating System mechanism responsible for decadal reversals of the Ionian basin-wide circulation (BiOS) (Gacic et al., 2011, 2014) as a pattern of Eastern Mediterranean climate change. The ROMS model successfully simulated the observed general circulation pattern in the Eastern Mediterranean. Over the period from July 1997 till December 2001, the Med-ROMS has successfully simulated the north Ionian inversion; SSHa same as Satellite SSH with an averaged RMSE between them of 0.0792 m. The spatial correlation maps between wind stress curl and Med-ROMS-SSHa/EOF1-SSHa are made and found to be significantly correlated at a 95% confidence limit. The highest significant correlation coefficient for Med-ROMS-SSHa was approximately 0.8 and located off the western Turkish coast inside the Aegean Sea. This strong significant positive correlation reflects the cyclonic motion of Rhodes Gyre. A high significant correlation coefficient for Med-ROMS-EOF1-SSHa, of around 0.51, was found along the western coast of Greece in the northeast Ionian Sea. For the first time, we could correlate the North Ionian Sea inversion to wind stress curl, which was significantly correlated with the EOF1 Med-ROMS SSHa averaged hindcasts during the inversion period. In this transient period, we noticed a significant correlation coefficient, at a 95% confidence limit, between NAO indices moving on average over 12 months and Med-ROMS-SSHa -PC1 over the Eastern Mediterranean.

1. Introduction

The Mediterranean Sea is a semi-enclosed basin surrounded by land with a single opening at the narrow Strait of Gibraltar connecting the sea to the Atlantic Ocean. It extends from 30° to 46°N and from 5°W to 36°E. The Mediterranean Sea basin is sub-divided into two sub-basins; the Western and Eastern Mediterranean basins, which are connected by the strait of Sicily. Balearic, Ligurian and Tyrrhenian sub-basins constitute the Western Mediterranean Sea, while the Ionian, Adriatic, Aegean and Levantine sub-basins make up the Eastern Mediterranean as shown in Fig. 1A. For the Mediterranean basin, there are three major meridional and zonal vertical circulation belts. The first is an open zonal vertical circulation belt that is shallow (0–500 m) and associated with the inflow of Atlantic Water at Gibraltar strait, transformed into Levantine Intermediate Water (LIW) in the Eastern Mediterranean. The LIW is an important component of the flow exiting from Gibraltar, and the Western Mediterranean deep waters also contribute to the bulk of the out flowing water masses see Fig. 1B. The other circulation belts are meridional cells driven by the deep-water mass formation processes occurring in the Northern Mediterranean areas, such as the Gulf of

* Corresponding author at: Marine Institute, Oranmore, Galway, Ireland.
E-mail addresses: hznagy@ims.metu.edu.tr, hazem.nagy@marine.ie (H. Nagy).

https://doi.org/10.1016/j.pocean.2019.04.012
Received 5 April 2018; Received in revised form 30 April 2019; Accepted 30 April 2019
Available online 02 May 2019
0079-6611/ © 2019 Elsevier Ltd. All rights reserved.

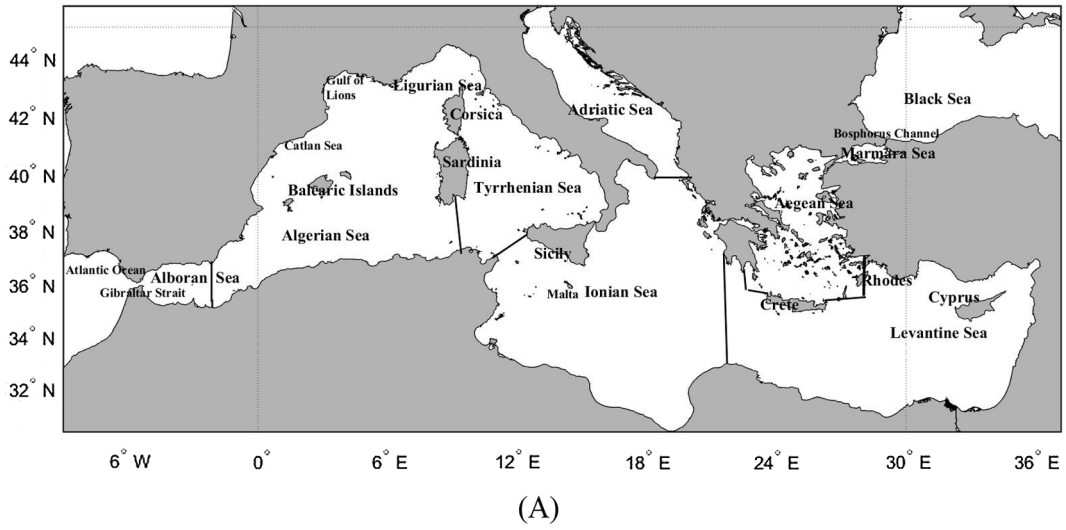

(A)

(B)

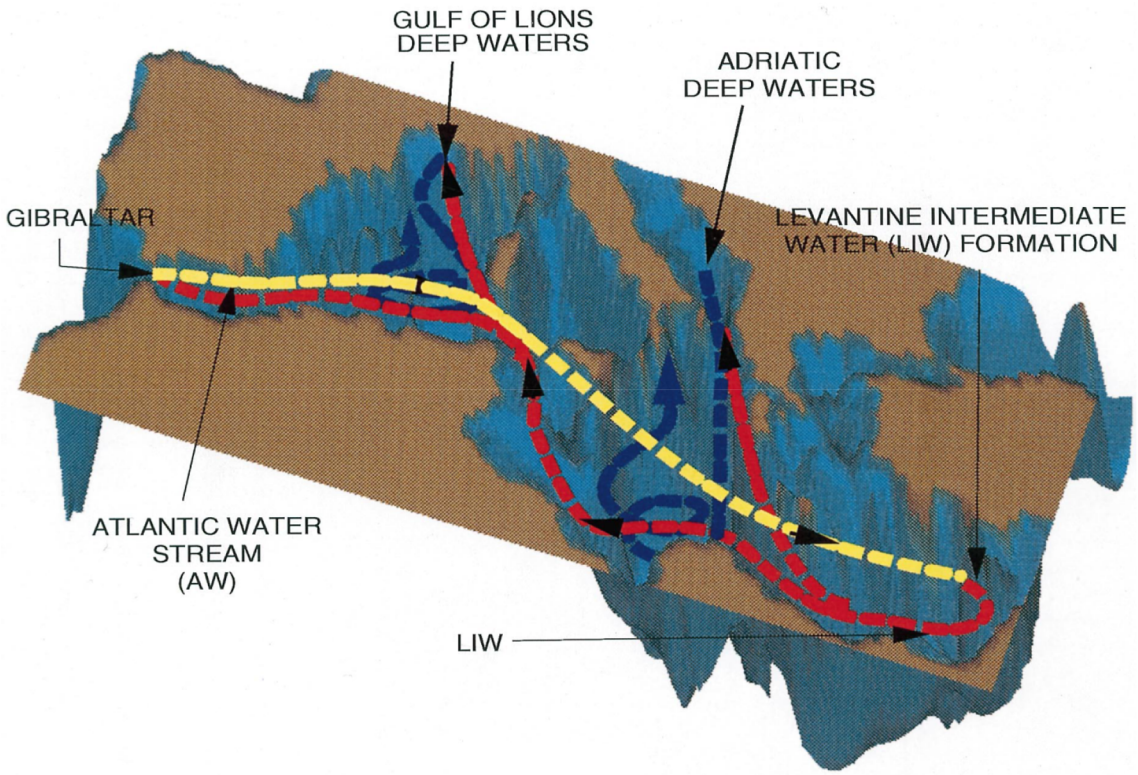

Fig. 1. (A) The Mediterranean Sea with the main geographic features and (B) Schematic map of the main water masses in the Mediterranean Sea according to Pinardi and Masetti (2000).

Lions and the Adriatic Sea to form the Gulf of Lions deep waters in the western part of the Mediterranean and the Adriatic Deep waters in the eastern part of the Mediterranean. The deep-water formation in such areas is not only affected by the presence of LIW, but also controlled by it. Thus, the meridional and zonal cells are interconnected into the Eastern and Western Mediterranean. The meridional overturning cells can communicate even at long time scales. The zonal cells have decadal timescales, while the meridional overturning cell has a multi decadal timescale (50–80 years) (Pinardi and Masetti, 2000). On the other hand, the inter-annual and decadal timescales of the spreading of these water changes is still unknown. Ocean modelling offers potential to capture the main features of this circulation, and are therefore instrumental in exploring the sensitivity of the Mediterranean Sea. There have already been a number of studies simulating the Mediterranean Sea region including Demirov and Pinardi, 2002; Pinardi et al., 2003; Beranger et al., 2004; Pinardi and Coppini, 2010; Adani et al., 2011 and Pinardi et al., 2015.

El-Gindy and Sharaf El-Din (1985), determined the percentages of Adriatic, Levantine and Cretan sea water types of the Eastern Mediterranean, using the triangle of mixing and the measured hydrographical variables (temperature and salinity), that verified the Cretan sea water percentage and their flow direction as a contributor to the deep waters in this region.

Roether et al. (1996) noticed that the Aegean Sea could be a source

of Eastern Mediterranean Deep Water, even larger than the most abundant source known to be located in the southern Adriatic Sea in the so-called Eastern Mediterranean Transient (EMT).

Tsimplis (2001) discovered that the strengthening of the NAO from the 1960s to the 1990s explains a significant proportion of the reduction in Mediterranean Sea level over this period.

Pujol and Larnicol (2005) studied the eddy kinetic energy (EKE) variability over the Mediterranean Sea using eleven years (1993–2003) of merged altimetry data (T/P, Jason, ERS and Envisat). They calculated the Mean Dynamic Topography (MDT) using the Rio et al. (2005) method to derive the absolute dynamic topography (ADT) over the Mediterranean Sea. The EKE variability in the Ionian suggested a reversal of the circulation in 1997. They observed a strong positive EKE trend, coupled with an increase in the seasonal cycle amplitude, during 1997 in the central Ionian basin. They also found a high correlation between wind stress variation and high-frequency EKE in the Ionian Sea.

Borzelli et al. (2009) studied the Eastern Mediterranean Transient and reversal of the Ionian Circulation. They carried out the study using satellite maps of Absolute Dynamic Topography (ADT) and Sea Surface Temperature (SST) over the Eastern Mediterranean covering the period from June 1993 until June 2001. They identified a complete reversal of the Ionian upper-layer circulation from anticyclonic to cyclonic by the middle of 1997. The inversion of the upper-layer circulation from anticyclonic to cyclonic could not have been explained in terms of the wind forcing. They concluded that the change in the observed upper circulation may be attributed to a baroclinic vorticity production.

Gacic et al. (2011) studied the impact of decadal inversions of the Ionian upper layer circulation as a mechanism called the Adriatic-Ionian Bimodal Oscillation System (BiOS). They showed cyclical occurrences of high salinity in the EMT and decadal reversals of the Ionian upper-layer basin circulation from cyclonic to anticyclonic and vice versa which was described in Gacic et al. (2014), Mihanović et al. (2015), Carniel et al. (2016), and Shabrang et al. (2016).

Pinardi et al. (2015) described the south-eastern Levantine surface circulation being as dominated by the Southern Levantine Current (SLC) indicating a decadal variability associated with the Northern Ionian reversal phenomenon.

Nagy et al. (2017) found that, the role of the wind stress on the dynamics of the south Levantine basin is crucial to force the circulation over that area.

1.1. Objectives of the study

Our main goal on this study is to identify the components in the variability of the Eastern Mediterranean Sea surface height and circulation, and to attribute them to observed physical processes. The Med-ROMS design, implementation and sensitivity studies will described in this paper. The EOF Analysis of sea surface height anomalies for satellite and Med-ROMS Hindcasts will be completed, and the reversal of the Ionian upper-layer circulation in the period 1997–1998 will be discussed. Further the correlation coefficients between the NAO index and EOF-SSHa Med-ROMS averaged hindcasts will be shown.

2. Model design and lateral boundary implementation

The model used in this study is the Med-ROMS ocean-modelling system, to explore the inter-annual and decadal dynamics of the Mediterranean Sea circulation and to assess the range of circulation structures response to climate change. It is a three-dimensional finite difference, free surface numerical model, utilizing the hydrostatic approximations with a time split mode algorithm for the internal and external modes. The Med-ROMS is a high- horizontal resolution (8.6 km) implementation and 30 sigma layers of the Regional Ocean Modelling System (Shchepetkin and McWilliams, 2005) for the Mediterranean Sea, developed at the Georgia Institute of Technology as a part of a joint international effort between Georgia Tech and the European Mediterranean Forecasting System (MFS) (Pinardi et al., 2003). The Med-ROMS is applied to simulate the seasonal and time-dependent simulation of the Mediterranean Sea over the period 2000–2006 using advanced data assimilation techniques based on variational methods (Vukicevic and Hess, 2000, Fukumori et al., 2004, Chhak and Di Lorenzo, 2007; Di Lorenzo et al., 2007). All the model equations are written in rectangular coordinates and contain spatially and temporally varying horizontal eddy viscosity and diffusion coefficients. The vertical mixing coefficients for tracers are calculated using the Mellor and Yamada, 1982, turbulence level 2.5 closure scheme.

The Med-ROMS bathymetry was extracted from the U.S. Navy unclassified bathymetric database (DBDB1), which has a horizontal resolution of one minute (1/60° × 1/60°). The model minimum depth was set at 10 m up to the coastline. In order to reduce the pressure gradient errors, we have smoothed the model bathymetry according to the rx_0 factor of Beckmanand Haidvogel (Haney, 1991). The dimensionless rx_0 factor of Beckmanand Haidvogel, is equal (difference of depths/sum of depths for two adjacent cells), which should not go

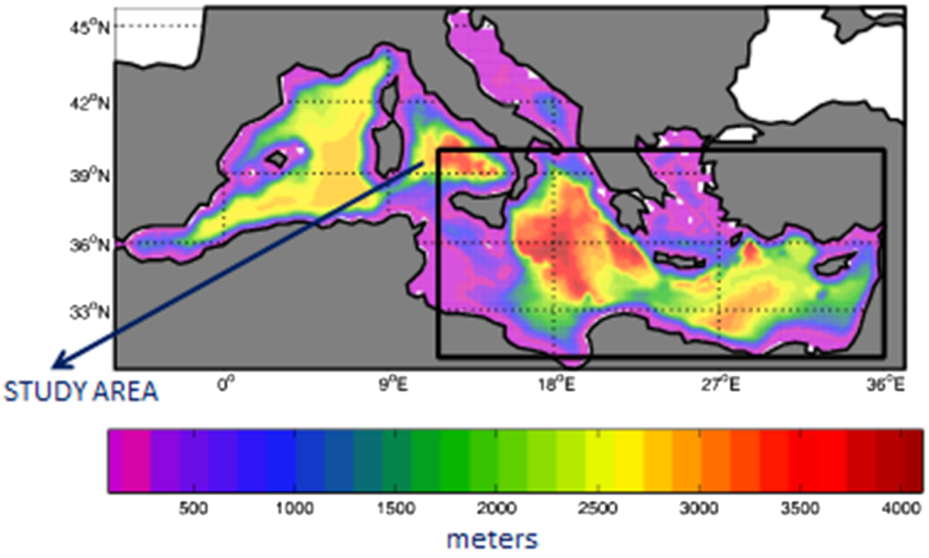

Fig. 2. Bathymetry of the Mediterranean Sea in meters according to Med-ROMS Model with a specification for the study area.

above 0.2. Then, we smoothed the bathymetry using the Laplacian filter. The study area with the interpolated bathymetry is shown in Fig. 2.

The physical forcing fields were provided by MFS-SYS2b ocean forecasting system that managed by CMCC Centre of Euro-Mediterrnean Climate Change, Bologna, Italy. This system was based on the OPA8.2 model (Madec et al., 1998) implemented for the Mediterranean Sea (Tonani et al., 2008) and includes the System for Ocean Forecasting and Analyses assimilation scheme (Dobricic et al., 2007). MFS-SYS2b has been intensively validated and represents one of the most advanced tools for the simulation of circulation in the Mediterranean Sea. The CMCC circulation model has supplied three and two-dimensional surface physical forcing fields for the whole Mediterranean Sea domain. The data sets are zonal, meridional and have vertical current speeds, vertical eddy diffusivity, temperature and salinity. The second are solar short-wave irradiance and wind speed. The three velocity components are necessary to calculate the transport term for each passive tracer. Eddy diffusivity is relevant to reproduce the vertical mixing processes of the tracers along the water column. The horizontal resolution of the climatological data for the whole Mediterranean Sea was 1/16° with 72 vertical z-levels.

The model has an open boundary condition at the Gibraltar strait. The Med-ROMS lateral boundary conditions were taken from the MFS-OGCM on the climatological basis. The lateral boundary fields were monthly averages from the MFS-OGCM SYS-2B perpetual year. The inputs are temperature, salinity, total velocity components, surface elevation and barotropic velocity components. The nesting has been designed to ensure that the volume transport across the open boundary of the nested model matches the volume transport of the MFS model.

For the barotropic velocity we use the Flather (1976) modified boundary condition discussed in Oddo and Pinardi (2008). At the outflow, we impose:

$$\bar{Un}_{nesed} = \left[\sqrt{\frac{g}{H_{nested}}}(\eta_{nested} - \eta_{nesting})\right] - \bar{Un}_{nested}\frac{H_{nesting} + \eta_{nesting}}{H_{nested} + \eta_{nested}} \quad (1)$$

where $\bar{Un} = \frac{1}{H+\eta}\int_{-H}^{\eta} Un\, dz$ is the normal barotropic velocity at the open boundaries and g the gravity, while at the inflow will be $\bar{Un}_{nesting} = \bar{Un}_{nested}$.

For the baroclinic velocity, we impose the normal velocity according to the following formula:

$$\int_{n2}^{n1}\int_{-H_{nested}}^{\eta_{nested}} Un_{nested}\, dz dn = \int_{n2}^{n1}\int_{-H_{nesting}}^{\eta_{nesting}} Un_{nesting}\, dz dn \quad (2)$$

where Un is the normal component to the open boundaries in m/s.

For the temperature and salinity, we use an upstream advection scheme whenever the normal velocity is directed outwards:

$$\frac{\partial T_{nested}}{\partial t} + Un_{nested}\frac{\partial T_{nested}}{\partial y} = 0\ ;\ \frac{\partial S_{nested}}{\partial t} + Un_{nested}\frac{\partial S_{nested}}{\partial y} = 0 \quad (3)$$

While on the inflow the temperature and salinity is prescribed to be identical to the interpolated MFS values. Where n_1, n_2 are the extremes of the open boundary section, $\eta_{nesting}$, $H_{nesting}$ are the surface elevation and the bathymetry of the nested model, while η_{nested}, H_{nested} are the surface elevation and bathymetry of the MFS model and Un is the normal velocity component to the open boundaries. The total tangential velocity at the open boundaries are set to be equal between the MFS and the nested model.

Finally, the nested model temperature and salinity fields have been nudged toward the MFS values in the right-hand side (r.h.s) of the prognostic fields following Marchesiello et al. (2001). Indicating temperature or salinity with 'gamma' we add a relaxation term such as:

$$\frac{\partial \gamma}{\partial t} = r.\ h.\ s - \frac{1}{\Gamma}(\gamma - \gamma^{MFS}) \quad (4)$$

Here Γ is the relaxation time that varies smoothly from ten model grid internal points to the open boundaries with values of 240 secs to 100 days. This nudging prevents a substantial model drift from the MFS values.

2.1. Sensitivity experiments and data

The sensitivity experiments that will be described in this section are listed in schematic Fig. 3 The model was spin-up for 50 years, using monthly climatological forcing provided from MFS-SYS2B climatology and restoring boundary conditions for surface temperature and salinity as shown in Fig. 3.

We used the previous year's spin-up model results as initial conditions for the 50-year control run. Both net heat and fresh water model fluxes were carefully corrected by using the new fluxes obtained from spin-up run plus, relaxation term obtained from MFS-SYS2b climatology see Eq. (4). This extra term, which has been extracted from MFS-SYS2b, sea surface temperature and sea surface salinity, was to control the simulation from drifting away the MFS climatological values. In addition, the water flux required a flux correction term, in order to impose a forcing that produces sea surface salinities consistent with the seasonal climatology and to avoid the excessive freshening or salting of the basin resulting by the use of the climatological forcing (Zavatarelli et al., 2002). The Med-ROMS heat flux and salt flux boundary condition during spin-up and control runs given by:

$$\rho_o C_P K_H \frac{\partial T}{\partial z}\bigg|_{z=\eta} = Q_T + \frac{\partial Q}{\partial T}(SST_{MFS\text{ - }SYS2b} - SST_m) \quad (5)$$

$$K_H \frac{\partial S}{\partial z}\bigg|_{z=\eta} = SSS_m(E - P) + \frac{1}{\gamma}(SSS_{MFS\text{ - }SYS2b} - SSS_m) \quad (6)$$

where Q_T is the total net heat flux according to the formula:

$$Q_T = Q_S - Q_b - Q_e - Q_h \quad (7)$$

The last terms in Eqs. (5) and (6) are the heat flux and salt flux correction terms, ∂Q/∂T is the heat flux correction in W/m^2 °C, SST_m and SSS_m are the model sea surface temperature and salinity, while SST_{MFS_SYS2b} and $SSS_{MFS\text{-}SYS2b}$ are the reference SST and SSS fields. Q_S, Qe, Q_b and Q_h are the short, latent, back and sensible heat fluxes in W/m^2. (K_H) is the vertical mixing coefficients for tracers in (m^2 s^{-1}). The relaxation time γ has been chosen to be equal to one day. E is the evaporation, P the precipitation, and w is the vertical velocity at the free surface elevation η in meters.

Our present study started at the end of the control run and after three hindcasting simulations were completed. Each one started at the end of the previous 50-year run that have been carried out, providing three ensemble members obtained from the corrected ERA-40 re-analyses (Pettenuzzo et al., 2010) covers the time period from January 1958 to December 2001. The atmospheric data for the computation of the surface forcing was obtained from the six hourly, 0.5° horizontal-resolution ECMWF surface analyses.

The atmospheric fields used are air temperature, dew point temperature, wind velocity at 10 m above sea level, mean sea level pressure, cloud cover and sea surface temperature. In order to parametrize the air-sea interaction processes, the wind stress, heat fluxes and evaporation rate are computed by means of interactive bulk formulae making use of atmospheric data including ECMWF sea surface temperature.

The momentum flux boundary condition for the surface takes the form:

$$\left(\rho_0 K_M \frac{\partial(u, v)}{\partial z}\right)_{z=\eta} = (\tau_{wx}, \tau_{wy}) \quad (8)$$

In Eq. (7), η is the free surface elevation in (m) and τ_{wx}, and τ_{wy} are the wind stress components in Nm^{-2}. The drag coefficient in Eq. (8) is computed according to Hellerman and Rosenstein (1983). (K_M) is the vertical mixing coefficient for momentum.

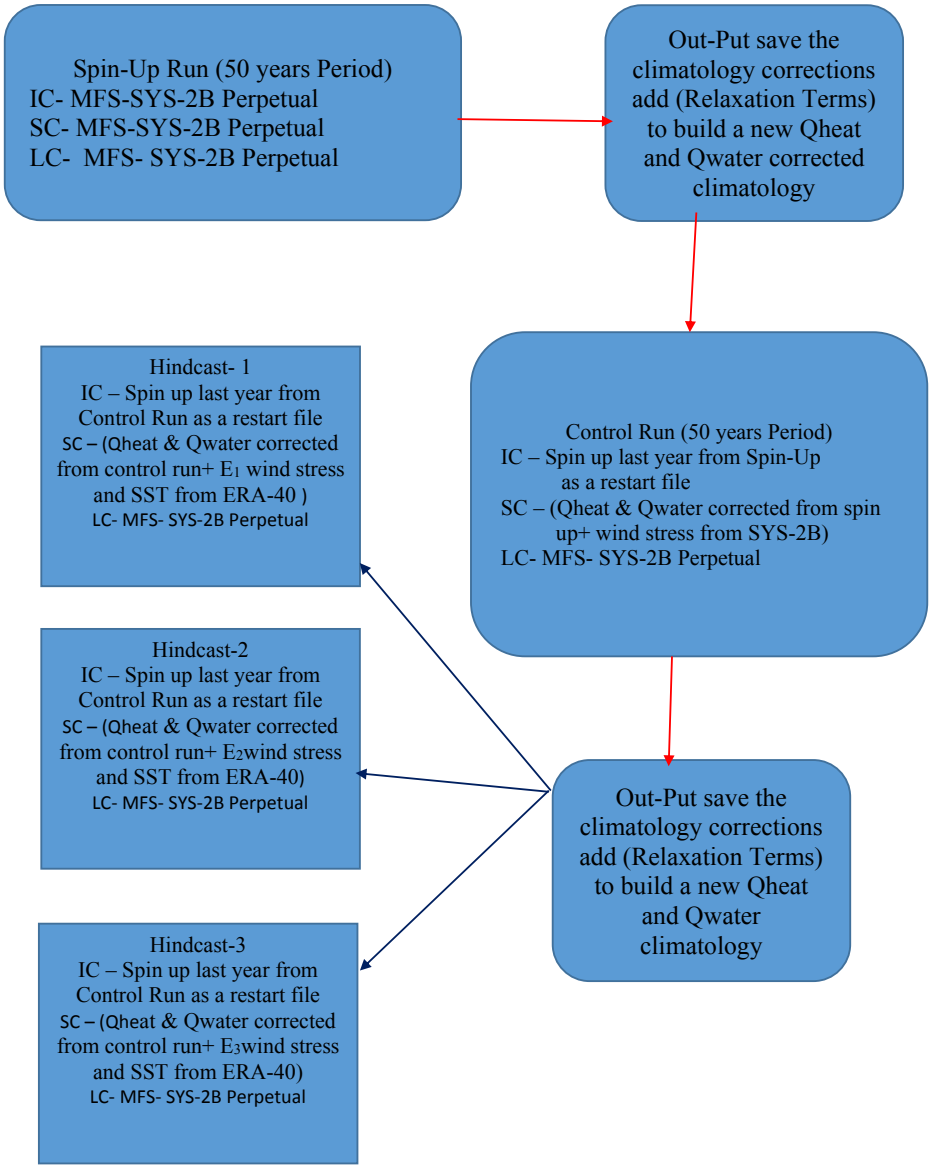

Fig. 3. Schematic of sensitivity experiments design for the Med-ROMS spin-up, control and hindcasts simulation over the period of January 1958 until December 2001.

The spatially dependent correction factors are applied to the basic atmospheric fields required as input to air-sea bulk formulae including radiation. These correction factors are obtained by comparison of the (ECMWF) Re-Analysis fields (ERA-40 (Uppala et al., 2005)) with satellite observations and in situ data sets available for the period 1985–2001. The corrections of ERA-40 surface flux products are consistent with the Mediterranean heat and water budgets and the connection between basin surface total heat flux and (NAO). The ERA-40 SST correction ranged from more than 2 °C to approximately −1 °C (Pettenuzzo et al., 2010). We have used three different ensembles obtained from MFS using Bayesian Hierarchical Models (BHM) to augment the Mediterranean Forecast of an ensemble ocean forecast methodology based on a surface wind BHM (MFS-Wind-BHM) described in Berliner and Kim (2007) and Milliff et al. (2011). A Bayesian hierarchical model (BHM) is developed to estimate surface vector wind (SVW) from ECMWF- ERA40 fields and associated uncertainties over the Mediterranean Sea. The three ensembles E_1, E_2 and E_3 have mainly produced from ECMWF ERA-40 wind velocity components. The differences between the three ensembles are relatively small regarding to variance terms in the SVW data-stage inputs from ECMWF. Our main aim from the choice of these three ensembles is to capture and ensure the dynamics of the SVW for most of the grid locations in the Mediterranean domain.

In spite of small differences between the members due to the model's internal variability, the main results do not change significantly when different members are considered. For the hindcast simulations, the heat fluxes are computed interactively according to Pinardi et al. (2003) the heat flux boundary condition is given by:

$$\rho_o C_P K_H \frac{\partial T}{\partial z}\bigg|_{z=\eta} = Q_T + \frac{\partial Q}{\partial T}\,(\mathrm{SST_{ERA\,-\,40}} - \mathrm{SST_m}) \tag{9}$$

$\mathrm{SST_{ERA\text{-}40}}$ is an ERA-40 reference SST field. While the model water flux boundary condition follows Beron-Vera et al. (1999) considering:

$$\mathrm{w}|_{z=\eta} = \left(\frac{\partial \eta}{\partial \mathrm{t}} + \vec{\nu}.\,\nabla\eta\right) + (\mathrm{E} - \mathrm{P}) \tag{10}$$

The corresponding model salt flux boundary condition is:

$$\mathrm{K_H}\frac{\partial \mathrm{S}}{\partial \mathrm{z}}\bigg|_{z=\eta} = SSS(\mathrm{E} - \mathrm{P}) \tag{11}$$

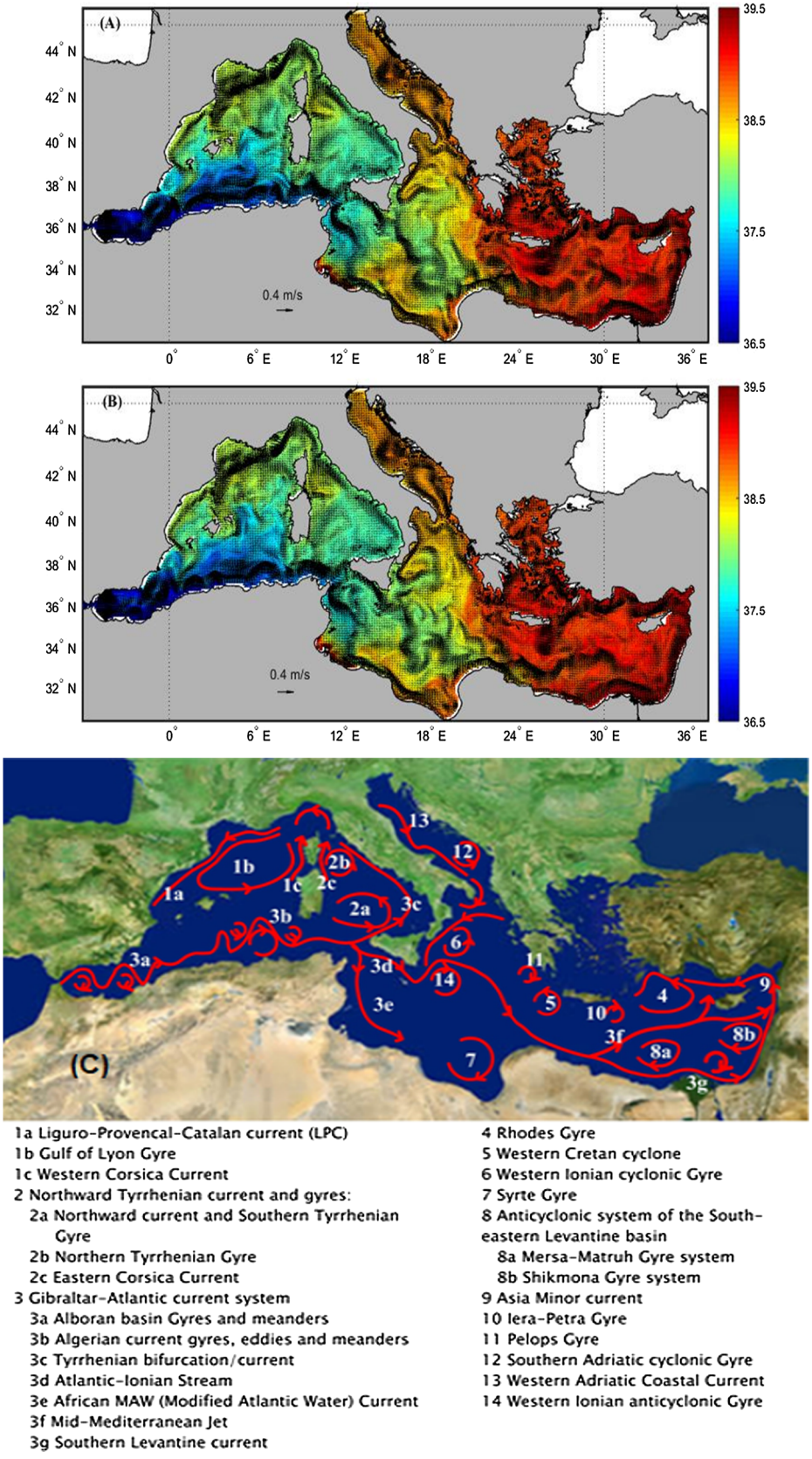

1a Liguro-Provencal-Catalan current (LPC)
1b Gulf of Lyon Gyre
1c Western Corsica Current
2 Northward Tyrrhenian current and gyres:
  2a Northward current and Southern Tyrrhenian Gyre
  2b Northern Tyrrhenian Gyre
  2c Eastern Corsica Current
3 Gibraltar-Atlantic current system
  3a Alboran basin Gyres and meanders
  3b Algerian current gyres, eddies and meanders
  3c Tyrrhenian bifurcation/current
  3d Atlantic-Ionian Stream
  3e African MAW (Modified Atlantic Water) Current
  3f Mid-Mediterranean Jet
  3g Southern Levantine current
4 Rhodes Gyre
5 Western Cretan cyclone
6 Western Ionian cyclonic Gyre
7 Syrte Gyre
8 Anticyclonic system of the South-eastern Levantine basin
  8a Mersa-Matruh Gyre system
  8b Shikmona Gyre system
9 Asia Minor current
10 Iera-Petra Gyre
11 Pelops Gyre
12 Southern Adriatic cyclonic Gyre
13 Western Adriatic Coastal Current
14 Western Ionian anticyclonic Gyre

Fig. 4. Near Surface salinity (5 m depth) and velocity [m/s] fields for Med-ROMS; (A) is Monthly averaged for the whole period of spin up and control run (100 years), (B) Monthly averaged Med-ROMS Hindcasts (1, 2, 3) over the simulation period January 1958–December 2001 and (C) Schema of the main circulation in the Mediterranean Sea according to Pinardi et al. (2005).

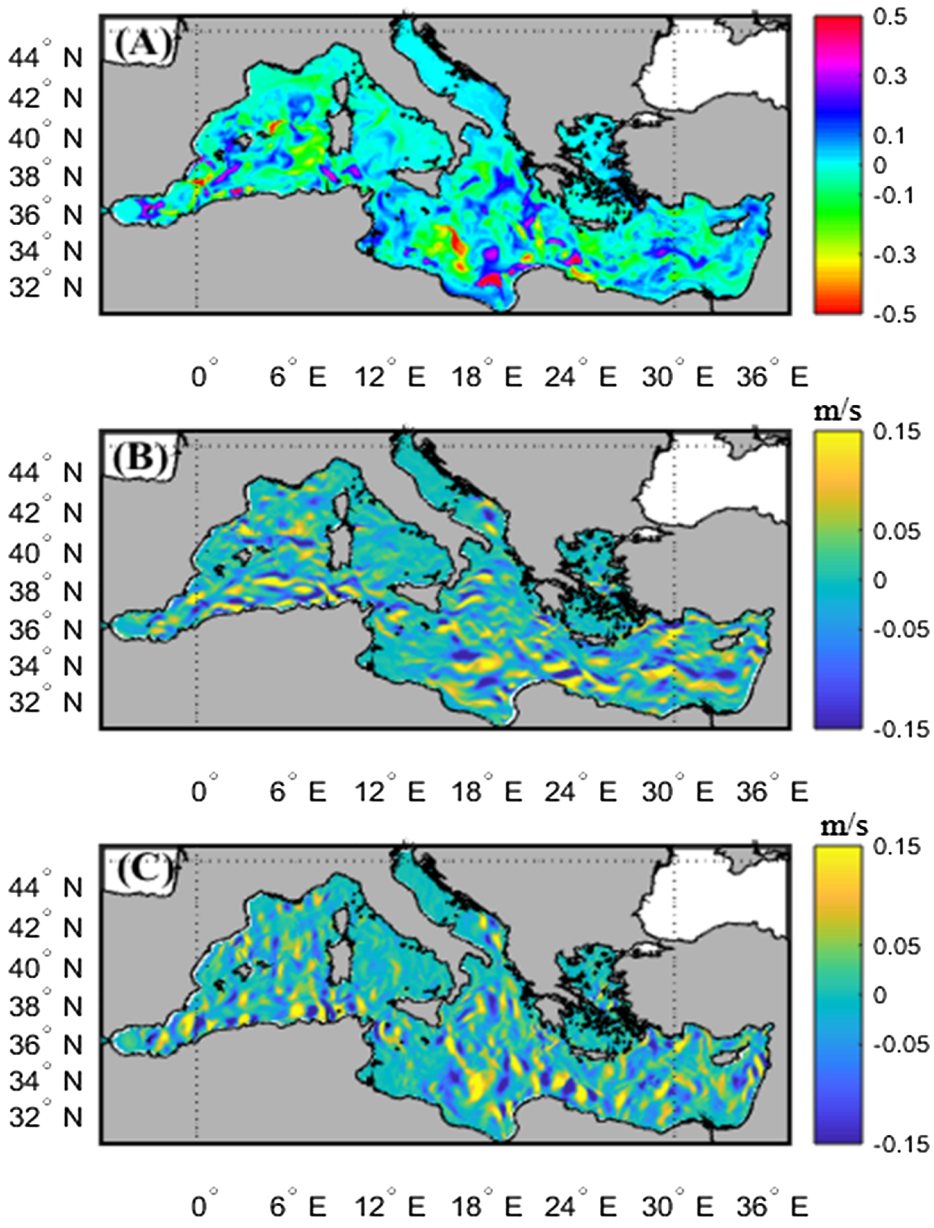

Fig. 5. Differences between monthly averaged Med-ROMS Hindcasts (1, 2, 3) over the simulation period January 1958–December 2001 and monthly averaged for the whole period of spin up and control run (100 years) (A) Near Surface salinity (5 m depth) (B) Velocity component U in m/s (C) Velocity component V in m/s.

SSS in Eq. (11) represents the Med-ROMS sea surface salinity. The average annual mean freshwater budget for hind casts simulation in the Mediterranean Sea, composed of evaporation minus precipitation has been found to be 0.456 m/year. This result is in agreement with Skliris et al. (2007), Sanchez-Gomez et al. (2011), Vervatis et al. (2013) and Verri et al. (2018), who found that the Mediterranean Sea net water surface flux to be 0.54 ± 0.15 m/year as a proposed annual average of several long-term estimates.

The focus of the article is Mediterranean Sea long term mean decadal circulation. For this reason the tidal forcing can be neglected according to Roussenov et al. (1995); Pinardi et al. (1997); Wu and Haines (1998); Korres et al. (2000) and Skliris et al. (2007) who made decadal simulations for the Mediterranean Sea circulation without including tidal forcing. Therefore, in this study the authors did not implement the tide in Med-ROMS.

Data used to validate the Med-ROMS include the altimetry observations of SSH derived from the Archiving, Validation, and Interpretation of Satellite Oceanographic data (AVISO) (Centre National d'Etudes Spatiales) https://www.aviso.altimetry.fr/en/home.html. Maps are used to validate aspects of Med- ROMS SSH. The AVISO maps that combine data from the TOPEX/POSEIDON, JASON-1, ERS-1/2, and Envisat satellites produce sea level anomalies at weekly resolution from October 1992 to December 2001 on a 1/3° × 1/3° Mercator grid (Ducet et al., 2000, Le Traon and Dibarboure, 1999). Here we use monthly averages of the SSH from the AVISO product for consistency. To verify that the model captures the main mesoscale variabilities we validate on the model grid.

This study used the monthly NAO index which obtained from the National Weather Service, Climate Prediction Center of NOAA (National Oceanic and Atmospheric Administration) (Barnston and Livezey, 1987). The data used covers the period from January 1958 to December 2001. The procedure used to identify the NAO index was rotated principal component analysis (Barnston and Livezey, 1987).

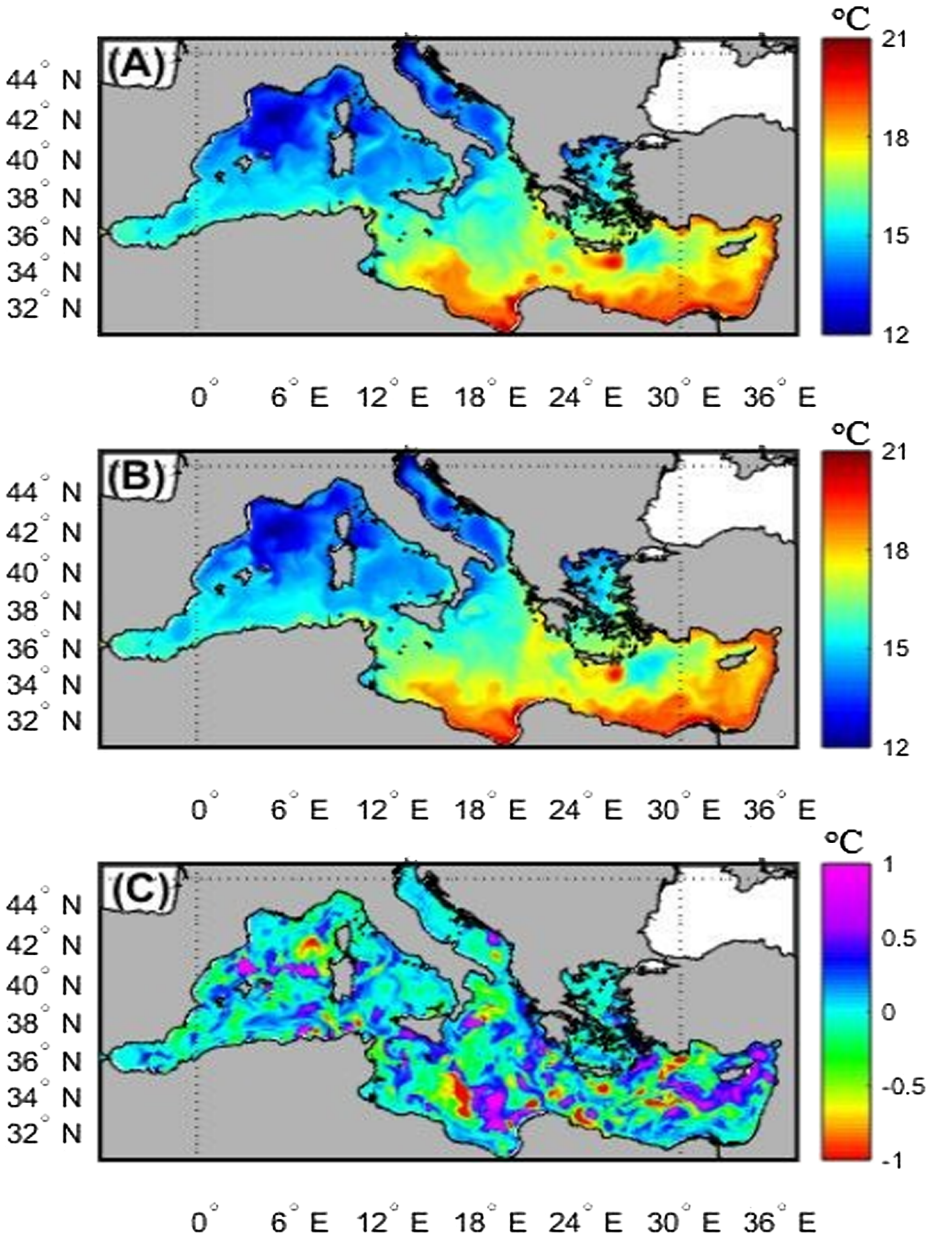

Fig. 6. Near Surface temperature (5 m depth) in [°C] fields for Med-ROMS; (A) is Monthly averaged for the whole period of spin up and control run (100 years), (B) Monthly averaged Med-ROMS Hindcasts (1, 2, 3) over the simulation period January 1958–December 2001 (C) Differences between Med-ROMS Hindcasts and spin up and control run (100 years).

2.2. EOF analysis

The Empirical Orthogonal Function (EOF) Analysis is a very powerful method when dealing with large amounts of data, to identify the principal modes in the variability and their overall contribution (Preisendorfer, 1988; Bjornsson and Venegas, 1997). The method constructs the initial data matrix F (x, t), where x is the space index and t are the time index, then calculates the covariance matrix $R = F^tF$ to find its eigenvectors and eigenvalues. This is a decomposition of the initial data. The eigenvectors are EOFs and each eigenvectors show the contribution of the corresponding eigenvalues to the variance (Bjornsson and Venegas, 1997).

3. Simulation results

In this section, we describe the major circulation features obtained from the spin-up, control and hindcasts simulations described in Fig. 3. Our aim in this section is to compare model results with the schematic of Pinardi et al. (2005) to verify the positions and the shape of the circulation with the monthly averaged model output.

The mesoscale eddies, identified /simulated by the Med-ROMS model, Fig. 4A, presents monthly averaged near surface salinity (5 m depth) and velocity [m/s] fields for the whole period of spin up and control run (100 years). While, Fig. 4 B shows the same previous fields of the monthly averaged Med-ROMS Hindcast (1, 2, 3) over the simulation period January 1958–December 2001. The circulation patterns and mesoscale features are well developed and clearer in Fig. 4(B) than in Fig. 4(A). The reason is that the spin-up and control simulations are using prescribed climatology fluxes from MFS products while the hindcasts one are using interactive fluxes from corrected ERA-40. Comparing our simulation results in Fig. 4(B) with Pinardi et al. (2005), schematic in Fig. 4C, which is based on observations, numerical modelling and satellites, some agreement can be shown in the main current system for the Eastern Mediterranean Sea such as the AIS (Atlantic

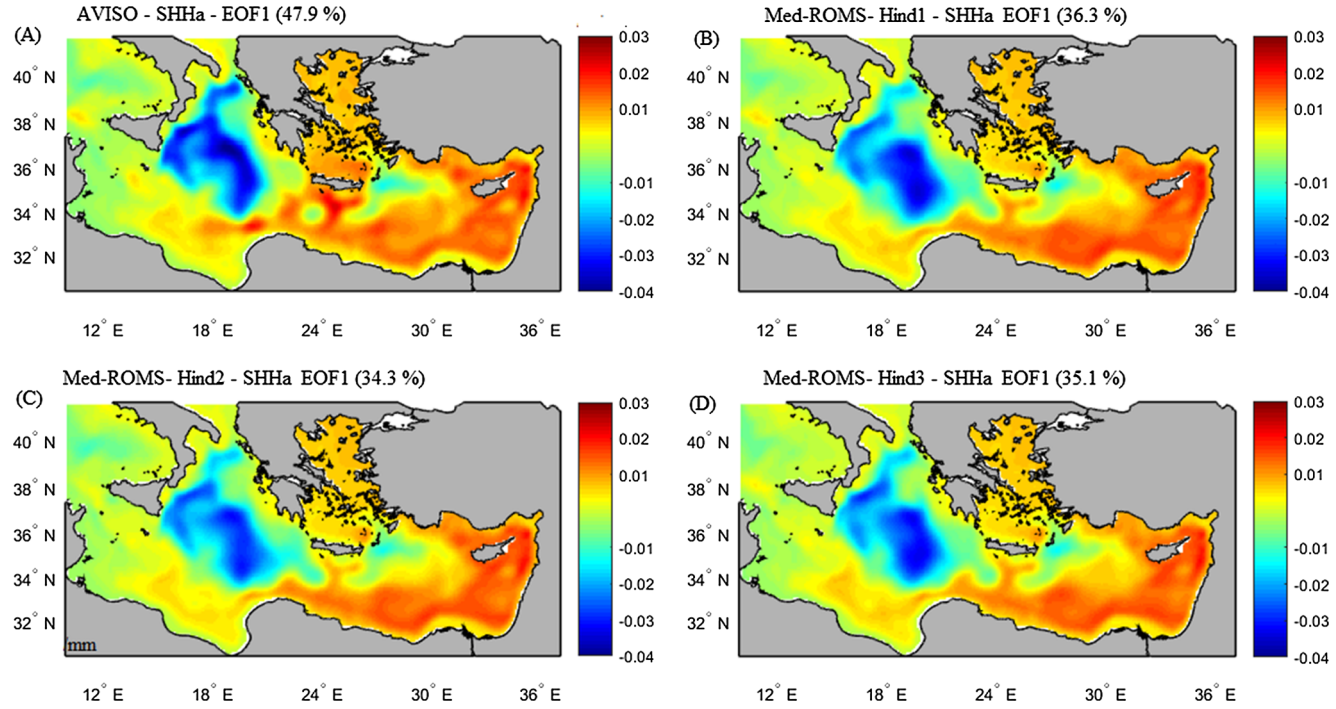

Fig. 7. Spatial distribution of the First Empirical Orthogonal Functions (EOF), (A) AVISO satellite sea surface height anomaly and (B–D) Med ROMS sea surface height anomalies for Hind1, Hind2 and Hind3 respectively.

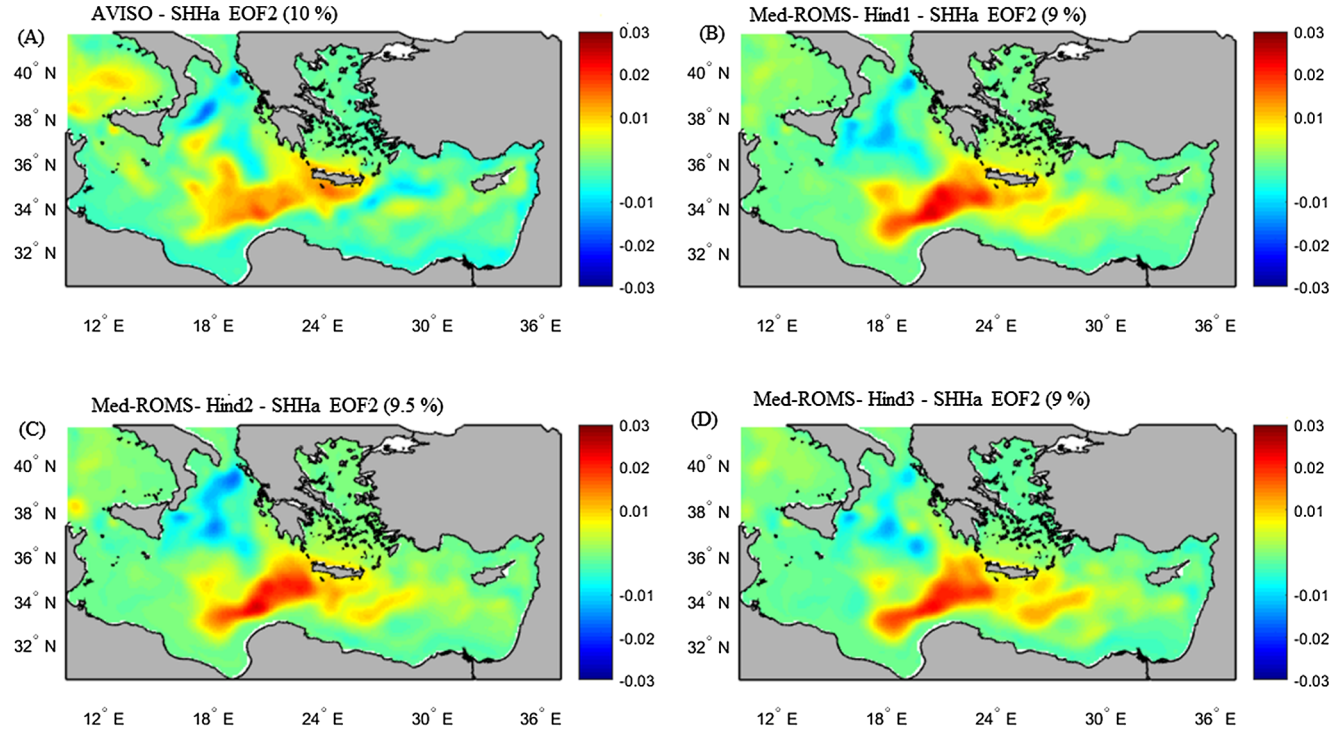

Fig. 8. Spatial distribution of the Second Empirical Orthogonal Functions (EOF); (A) AVISO satellite sea surface height anomaly and (B–D) Med ROMS are sea surface height anomalies for Hind1, Hind2 and Hind3 respectively.

Ionian System), MMJ (Mid-Mediterranean Jet) and AMC (Asian Minor Current) in addition to the locations of some major mesoscale features such as Iera-Petra anticyclonic gyre, Shikmona, Rhodes, Pelops, Western Ionian cyclonic gyre, Mersa-Matruhanticyclonic gyre and Syrt gyre, which are found at the South-Eastern part of the Ionian Sea. On the other hand, the Med-ROMS monthly averaged hindcasts could not replicate the western Cretan cyclonic gyre in Ionian Sea. However, the results of Pinardi et al. (2005) are due to full monitoring system on the Mediterranean Sea from observation, satellites and modeling, while the Med-ROMS averaged hind casts are based on MFS temperature and salinity fields with surface fluxes from ERA-40 corrected. The output of the spatial salinity fields of the model of the Mediterranean Sea is shown in Fig. 4A and B. It suggests that AW (Atlantic Water), that enters the Gibraltar strait to the south of the African Coast, continues to the

Fig. 9. Temporal evolution of the basin averaged plotted standard deviation units (A). The first Principal Components (PC) for the Med-ROM SSSHa hindcast 1, 2 and 3 are shown in red, blue and green respectively, covering the period from January 1958 till December 2001 while AVISO Satellite PC SSHa is shown in black line covering the period from October 1992 till December 2001. (B) The second Principal Components (PC) for the Med-ROM SSSHa hindcast 1, 2 and 3 shown in red, blue and green respectively, covering the period from January 1958 till December while AVISO Satellite PC SSHa are shown in black line and covering the period from October 1992 till December 2001. (For interpretation of the references to colour in this figure legend, the reader is referred to the web version of this article.)

Sicily Channel towards the north, generating several mesoscale features in the Ionian Sea such as Western Ionian cyclonic gyre (38°N, 17.5°E) and Pelops anticyclonic gyre. This is in agreement with Pinardi et al. (2005).

In summary, the circulation patterns are showing the robustness of the model in reproducing the main general characteristics of the EMED (Eastern Mediterranean) and very rich in mesoscale features. Fig. 5A, B and C are the differences between monthly averaged Med-ROMS Hindcasts (1, 2, 3), over the simulation period January 1958–December 2001, and monthly averaged for the whole period of spin up and control run (100 years), for the salinity and velocity components. We have found the salinity difference between two simulations is maximum (0.47) in front of the Libyan Coast and inside Gulf of Syrt as shown in Fig. 5(A). This may be attributed to the poor data coverage along the Libyan Coast. The basin averaged RMSE between the two simulations was only 0.106 PSU. While the maximum velocity components differences between the two simulations are approximately ± 0.15 m/s.

Fig. 6A, shows the monthly averaged near surface temperature (5 m depth) for the whole period of spin up and control run (100 years). Fig. 6B suggest the same previous fields of the monthly averaged Med-ROMS Hindcast (1, 2, 3) over the simulation period January 1958–December 2001, while Fig. 6C is the differences between them. We can observe similarities in the positions and shapes of mesoscale features; for example the Gulf of Lyon gyre, southern Adriatic cyclonic gyre, Iera-Petra anticyclonic gyre, Shikmona, Rhodes, Pelops and Western Ionian cyclonic gyre. Fig. 6B shows an intense downwelling is observed at Longitude (27°E), a strong sign of Iera-Petra anticyclonic gyre. This semi-recurrent mesoscale feature is a relatively intense anticyclonic eddy located southeast of Crete Island (34°N, 27°E) (Burnett et al., 1991; POEM Group, 1992). There is a general agreement about the hypothesis that Iera-Petra is due to the curl imposed to the Etesians by the Crete Orography (Horton et al. 1994). Lascaratos and Tsantilas

Table 1
Correlation coefficients between Med-ROMS-SSHa Hindcasts EOF components (PC1 and PC2) with the satellite observations, (All values are significant at 95% confidence limit).

Simulation Name	Correlation Coefficients, between Med-ROMS-SSHa Hindcasts EOF components and the satellite observations (All values are significant at 95% confidence limit)	
	PC1	PC2
Hind-1	0.985	0.837
Hind-2	0.970	0.785
Hind-3	0.980	0.836

(1997), who analyzed 155 weekly infrared images in the period July 1993 to June 1996, found that Iera-Petra had undergone an annual cycle with some inter-annual variability. This may be due to the Med-ROMS hindcast simulations provided with corrected momentum and surface fluxes obtained from ERA-40 corrected ensembles as described in Section 2. Fig. 6C suggests that the highest differences between simulations was about ± 1.0 °C located off the Libyan coast and inside the Levantine Basin. This may be due to that the Hindcasts simulations are using particular surface flux parameterization (ERA-40 SST) as explained previously in Eq. (9). The RMSE basin averaged between the two simulations for the temperature is 0.1505 °C.

4. Comparison of EOF analysis of Sea surface height anomalies for satellite and Med-ROMS Hindcasts.

In the Eastern Mediterranean Sea, Fig. 7B, C and D show the Med-ROMS (SSHa) anomalies first EOF for Hind 1, 2 and 3 over the simulation period from January 1958 to December 2001, to be compared with altimetry data SSHa first EOF for the period from October 1992 to December 2001 in Fig. 7A. The anomalies are defined by deviation of the SSH from the climatic mean in the given month over the whole period of study. There is a significant resemblance in the spatial structure of the EOF first mode between the Med-ROMS Hind 1,2 with the EOF1 of satellite SSHa (Fig. 7A). Both EOF1s' relations, corresponding to a dipole, are easily recognized from the large negative values of SSHa (cooling) off the northern Ionian Sea and the large positive (warming) off the middle and east of the Levantine Basin. The first mode of variability of satellite and Med-ROMS Hind 1, 2, 3 SSHa explains 47.9%, 36.3%, 34.3% and 35.1% of the SSHa variance respectively. The EOF2 spatial patterns for both satellite and Med-ROMS Hindcasts SSHa are shown in Fig. 8A, B, C and D. EOF2 field corresponds to a dipole located in the Ionian Sea with maximum off the south Ionian Sea and minimum off the north Ionian Sea. The second mode of variability of satellite and Med-ROMS Hind 1, 2 and 3 SSHa explains 10%, 9%, 9.5% and 9% of the SSHa variance respectively. The temporal variability of SSHa PC1 for both Satellite and Med-ROMS Hindcasts is shown in Fig. 9A. It can be noticed that the Med-ROMS

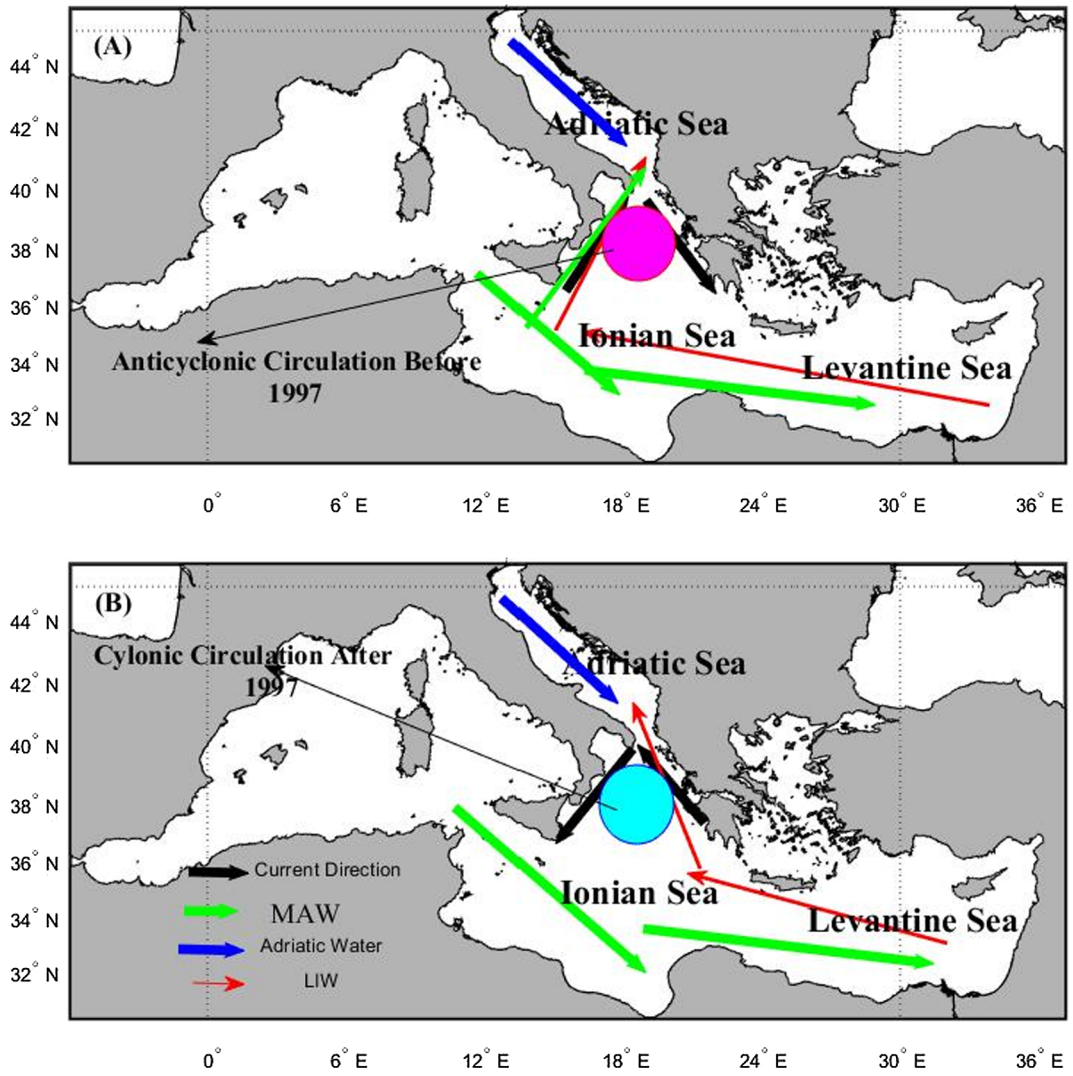

Fig. 10. Description of the BiOS mechanism (A) before1997 (B) after 1997, where the MAW is the Modified Atlantic water and LIW is Levantine Intermediate Water.

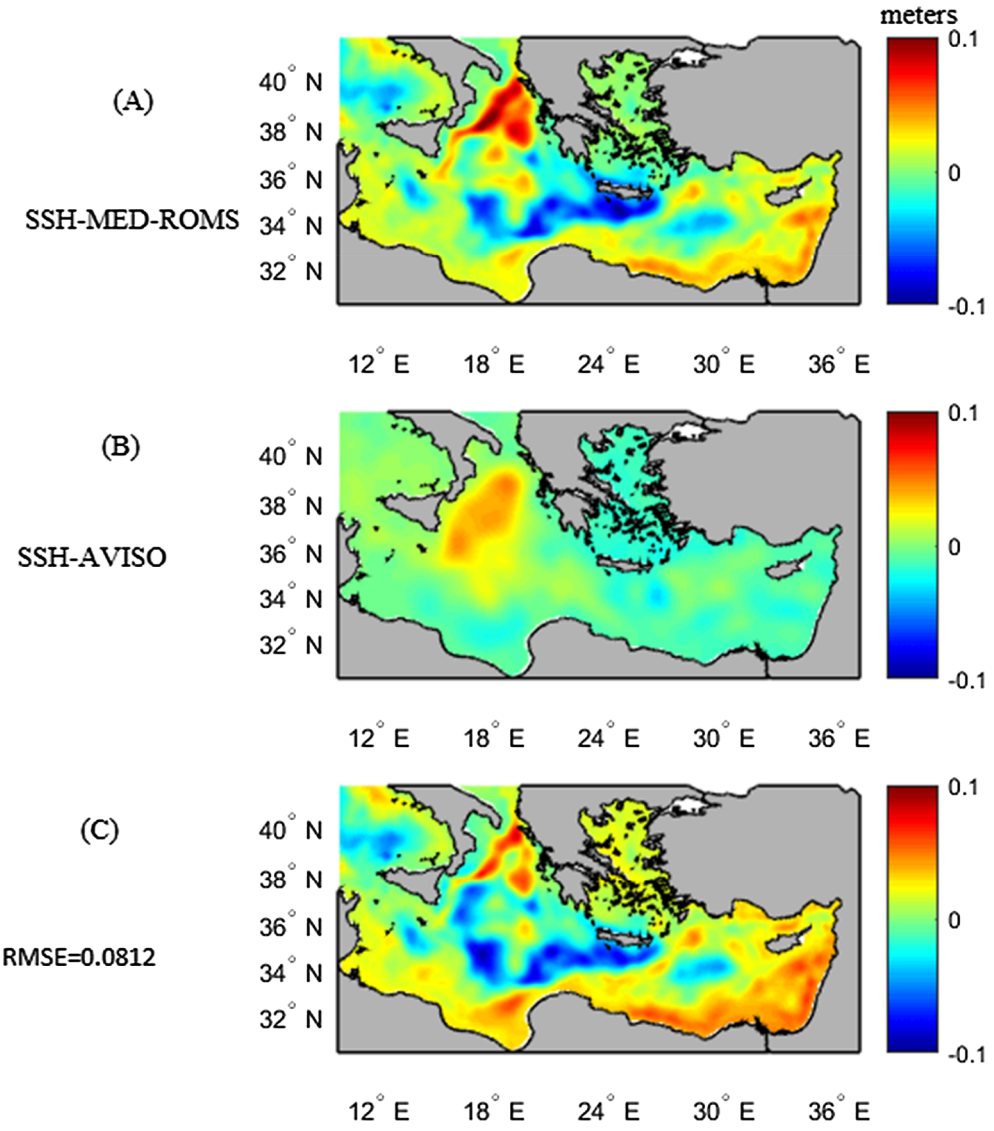

Fig. 11. Time averages of Sea Surface Height SSH in meters: (A) Averaged Med-ROMS Hindcast (1, 2, 3) in the period October 1992–June 1997, (B) Average of AVISO satellite in the period October 1992–1997 and (C) The difference between averaged Med-ROMS Hindcast (1, 2, 3) and AVISO satellite. The RMSE between them is 0.123 m.

Hindcasts PC1 is highly correlated with the satellite one. The correlation coefficients between Med-ROMS PC1 SSHa Hind 1, 2 and 3 and satellite observations are shown in Table 1. The correlation coefficients values are 0.985, 0.97 and 0.98 respectively and all values are significant at a 95% confidence limit. Fig. 9A, shows a strong positive signal during the 1998–1999 period. This strong signal may be associated with the relaxation of the Eastern Mediterranean Transient (EMT). This phenomena took place by the middle of 1997 and consisted of a complete reversal of the Ionian upper-layer circulation from anticyclonic to cyclonic according to, Pujol and Larnicol (2005), Gertman et al. (2006), Borzelli et al. (2009), Mihanović et al. (2015), Pinardi et al. (2015), Carniel et al. (2016), and Shabrang et al.(2016). Fig. 9B shows the temporal variability for PC2. Although the second mode of variability of satellite and model SSHa explains only 10% and 9% of the SSHa variance respectively, the model SSHa compares well with satellite SSHa variability. The correlation coefficients between Med-ROMS PC2 SSHa Hind 1, 2, 3 and satellite observations are presented in Table 1. The values are 0.837, 0.785 and 0.836 respectively and all values are significant at a 95% confidence limit. Again, we can recognize a clear high positive peak for the satellite PC2 SSHa but this time in the middle of 1997, while the Med-ROMS output indicates the same peak in 1998. Again, this strong positive signal may be attributed, to the EMT. An interesting strong negative signal is observed in early 2001 for both PC2 as shown in Fig. 9(B); this could be evidence of the time variability of the SLA pattern in the EMED during the year 2001. Overall, the Med-ROMS has significant skill in reconstructing the regional oceanic physical conditions and tracking the observed spatial and temporal fluctuations of SSHa from 1958 to 2001.

5. The 1997–1998 reversal of the Ionian upper layer circulation

This section describes the 1997–1998 reversal of the Ionian upper layer circulation, from anticyclonic to cyclonic, using Med-ROMS hindcast and AVISO satellite monthly averaged SSH. We outline the role of wind stress curl and correlate model first EOF1 SHHa with the averaged wind vorticity.

This phenomena is known as the Bimodal Oscillating System (BiOS) mechanism responsible for decadal reversals of the Ionian basin-wide circulation (Gacic et al., 2011, 2014). The BiOS mechanism can be described as follows with reference to Fig. 10A and B. Fig. 10(A) describes the circulation in North Ionian Sea before 1997, suggesting the low-salinity of MAW advected by the anticyclonic circulation entering

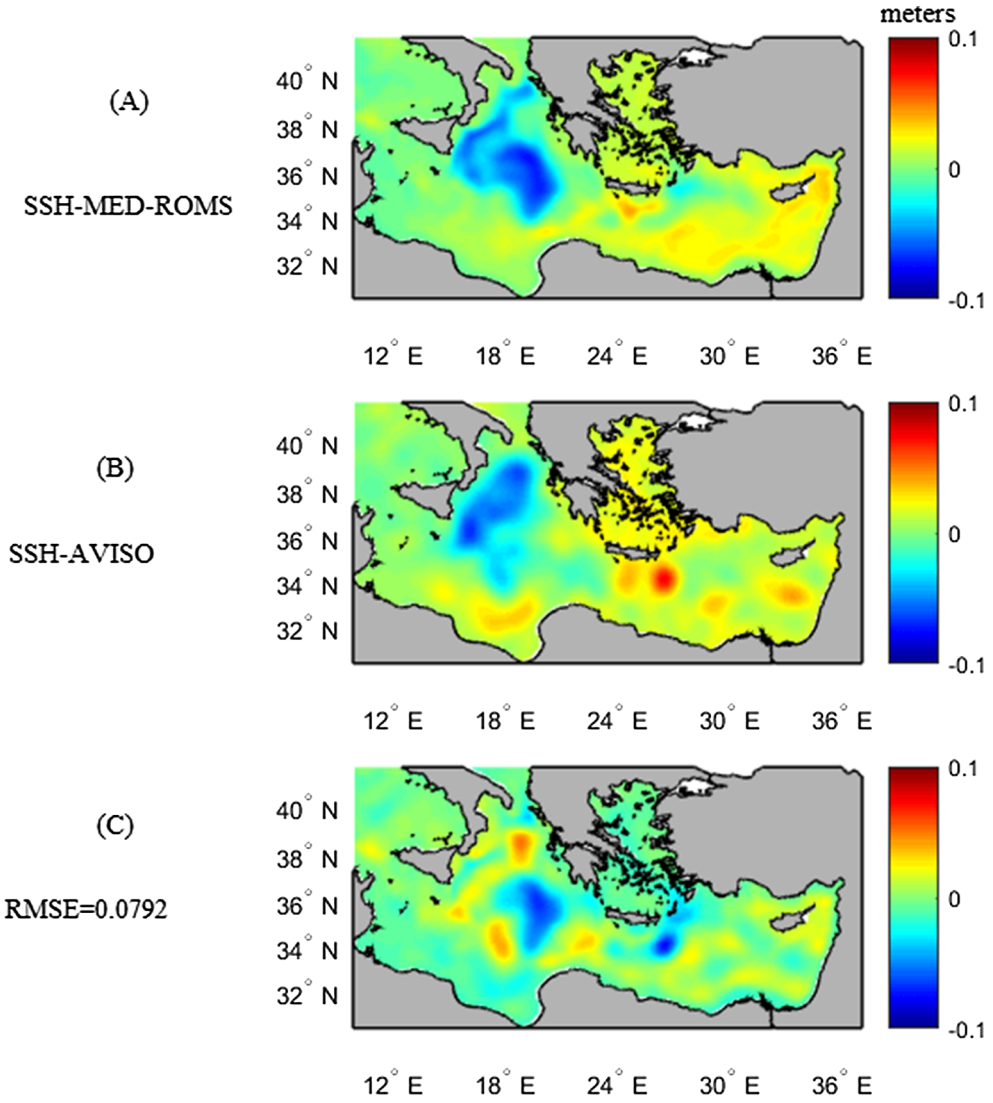

Fig. 12. Time averages of SSH in meters, (A) Averaged Med-ROMS Hindcast (1, 2, 3) in the period July 1997–December 2001, (B) Average of AVISO satellite in the period July 1997–December 2001 and (C) The difference between averaged Med-ROMS Hindcast (1, 2, 3) and AVISO satellite. The RMSE between them is 0.0792 m.

the Adriatic basin. It is important to underline that the anticyclonic trend advects mostly MAW, since the pathway followed by waters is towards the western border of the Ionian Sea (Civitarese et al., 2010; Crisciani and Mosetti, 2016). While after 1997 the cyclonic circulation over the north Ionian regime favors LIW (Levantine intermediate water) to enter the Adriatic, which are salty deep waters going into the Adriatic Sea (Fig. 10B). However, the denser Adriatic deep water spreads along the Ionian flanks increasing their density (Mihanović et al., 2015; Crisciani and Mosetti, 2016). After 1997, a cyclonic gyre is observed and this favors salty Levantine or Cretan water to enter, inverting the salt content of the Adriatic Deep Water (Carniel et al., 2016; Shabrang et al., 2016).

It is crucial for our study to provide an important case study such as BiOS by comparing the differences in upper Eastern Mediterranean circulation simulated by Med-ROMS hindcasts with AVISO Satellite SSH. This comparison will prove the quality of Med-ROMS in reproducing the main decadal reversals in circulation. The changes associated with the 1997–1998 North Ionian reversal in the Med-ROMS hindcasts are followed by comparison between the period before the shift (P1, October 1992–June 1997) and a period after the shift (P2, July 1997–December 2001) with the same for AVISO Satellite SSH. The chosen two periods are based on AVISO satellite SSH data availability, commencing in October 1992.

Fig. 11A, B show the comparison between the averaged Med-ROMS hindcast (1, 2 and 3) SSH over the period October 1992–June 1997 (P1) and the corresponding averaged AVISO satellite SSH for the same period. While Fig. 11C presents the differences between Med-ROMS and AVISO Satellite SSH with the corresponding RMSE. There is clear similarity between Fig. 11A and B in terms of the circulation pattern in the north Ionian Sea. The anticyclonic motion pattern is well represented in both Med-ROMS model and AVISO Satellite SSH but a much stronger Med-ROMS averaged hindcast is observed. There are some differences observed at the middle and eastern part of the domain as shown in Fig. 11C. In general, the Med-ROMS has lower SSH values than satellite observations in middle of the domain while higher SSH values are seen at the eastern part of the Levantine basin. The RMSE difference between the Med-ROMS SSH and AVISO satellite SSH was 0.0812 m averaged over the domain. This may be explained by the low frequency atmospheric variability in the surrounding basins and the relative coarse spatial resolution of the atmospheric forcing with AVISO data, which is challenging for the model oscillator dynamics to capture. Fig. 12A, B and C show the comparison between averaged Med-ROMS hindcasts SSH and AVISO satellite SSH with the difference between them over time period P2. Note the resemblance between the two maps

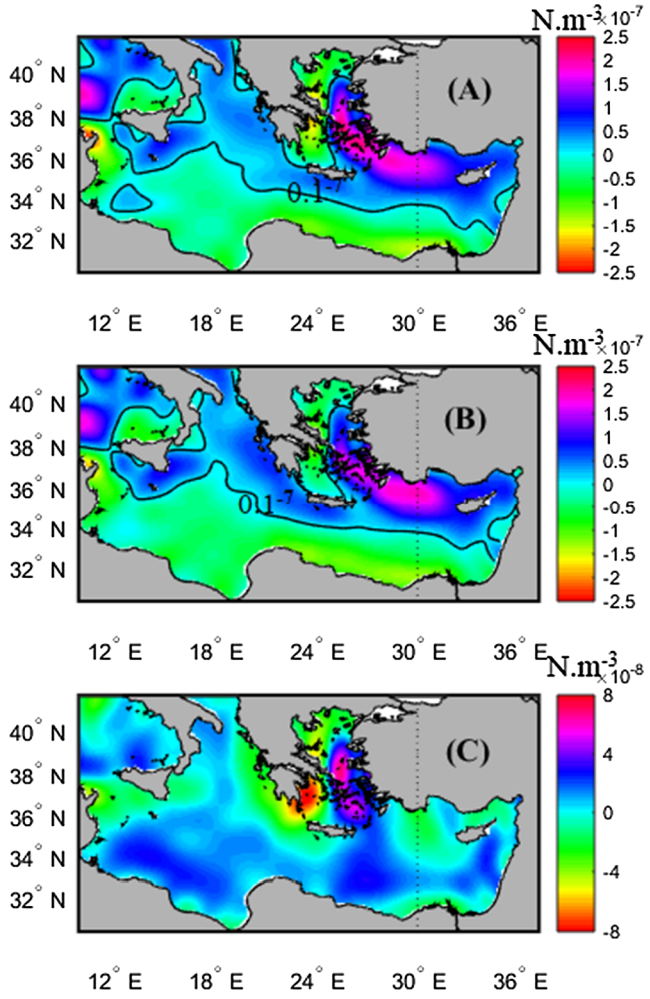

Fig. 13. Time averages of wind stress curl in N m^{-3}. (A) Averaged ERA-40 corrected ensembles (1, 2, 3) over the period October 1992–June 1997 and (B) Averaged ERA-40 corrected ensembles (1, 2, 3) over the period July 1997–December 2001 (C) Differences between P1 and P2 in N m^{-3}.

(Fig. 12A and B) in the position and the shape of the north Ionian cyclonic circulation. The Med-ROMS averaged SSH hindcasts observed during the north Ionian inversion are in agreement with Pujol and Larnicol (2005); Borzelli et al. (2009); Gacic et al. (2014). The difference between Med-ROMS SSH and AVISO satellite over P2 is a little lower than for P1; the SSH averaged RMSE between Med-ROMS and AVISO satellite is 0.0792 m.

5.1. Correlations between SSHa, first and second mode of EOF-SSHa Med-ROMS and averaged hindcasts and wind stress curl.

This section discusses the role of the wind stress curl in Bimodal Oscillating System mechanism responsible for decadal reversals of the Ionian basin-wide circulation (BiOS). Fig. 13A, B and C are the monthly averaged wind stress curl over P1, P2 and the differences between them (P1-P2) respectively. The positive wind stress curl sign is responsible for cyclonic motion while the negative is responsible for anticyclonic motion. The contour line in both figures distinguishes between positive and negative wind stress curl sign. Both wind stress curl patterns suggest prevalent cyclonic motion in the north-eastern Mediterranean areas while the opposite is occurring in the southern areas of the Mediterranean Sea in agreement with Pinardi and Masetti (2000) and Demirov and Pinardi (2002). There is a slightly higher wind vorticity in the North Ionian region over P2 see Fig. 13B than the same region over P1. This could be an explanation for the dominant cyclonic motion in north Ionian region over the whole period of P2. Fig. 13C suggests an interesting strong minimum negative difference value, of about -8×10^{-8} N m^{-3}, along the Eastern Grecian Coast while a maximum difference occurs at the middle of Aegean Basin.

The correlation maps are made and significantly correlated at a 95% confidence limit. The significance test has showed the minimum significant correlation coefficient was about 0.1 at 95% confidence limit. Fig. 14A and B present the correlation between the wind vorticity and Med-ROMS averaged SSHa Hindcasts over the period P1 and P2. The highest significant correlation coefficient for both periods was around 0.8 located along the western Turkish coast inside the Aegean Sea and beside Rhodes Island. The significant positive correlations are reflecting the cyclonic motion of Rhodes Gyre. Another high positive correlation area found along the Tunisian Coast in the Ionian Sea as shown in Fig. 14A and B. It is obvious from Fig. 14A, at the North Ionian Sea area over the period P1, that the wind stress curl is significantly correlated with the Med-ROMS SSHa averaged hindcasts with correlation coefficient of about 0.6. While this significant correlation has dropped over P2 to be about 0.3. This may explain the motion inversion over P2. We can observe a strong negative correlation of about −0.8 over the Tyrrhenian Sea in both periods. Fig. 14B suggests small high positive correlations regions appeared in the Levantine Sea. This positive correlation could be a sign for possible cyclonic motion appeared in this regions over P2. In order to gain better insight about the inversion phenomena, we have calculated the correlation between the wind vorticity and Med-ROMS averaged EOF1 SSHa Hindcasts over the period P1 and P2 as shown in Fig. 15A and B. The highest correlation coefficient was about 0.51 along the western coast of Greece in the north east Ionian Sea. The contour line of 0.1 is differentiating between significant and non-significant correlation coefficients. In general, the EOF1 along the northern parts of the eastern Mediterranean Sea are significantly correlated with the wind stress curl over the period P1, except off the south-eastern Italian coast and the middle parts of the Aegean Sea as shown in Fig. 15A. The significant positive correlations are reflecting the cyclonic motion, principally due to positive wind vorticity. We can observe in Fig. 15A, two interesting areas of high negative significant correlation. The first one is located north of Crete Island while the other one off the Gulf of Syrt; this refers to the anticyclonic motion of the western Cretan gyre and Gulf of Syrt gyre. Fig. 15A and B show some differences in the coverage area of significant positive correlation innorth Ionian Sea. It is clear from Fig. 15B that at the North Ionian Sea area over the period P2, that the wind stress curl is significantly correlated with the EOF1 Med-ROMS SSHa averaged hindcasts. This explains the cyclonic motion in the north Ionian, observed in Fig. 12A, during the same period. We believe that using the ERA-40 corrected made by Pettenuzzo et al. (2010) and momentum flux ensembles Milliff et al. (2011), have reduced the model uncertainties errors. We noticed in Fig. 15B a high significant negative correlation off the Israeli coast about −0.45. This may be an indication of the circulation inversion first described by Pinardi and Navarra (1993). Fig. 16A and B are describing the correlation between averaged Med-ROMS EOF2-SSHa and wind stress curl over P1 and P2 respectively. The two maps suggest significant correlations in most of the Eastern Mediterranean but with less correlation values compared with EOF1-SSH-a. Fig. 11 A identifies two regions with high correlation coefficient values; south of Cyprus (R = 0.41) and south of Rhodes (0.39). The strong sign of the Rhodes cyclonic gyre is obvious in EOF1 and EOF2 over both periods, P1 and P2. This gyre is highly correlated with the wind vorticity. Therefore, the wind is playing an important role on the gyre existence agreeing with Pinardi and Navarra (1993), Lascaratos and Nittis (1998) and Theocharis et al. (1999). The highest correlation over P2 was found in Aegean Sea (R = 0.38) to the north of Crete Island. However, there is no significant correlation found in the north Ionian between Med-ROMS-EOF2 and the wind curl over both periods P1 and P2.

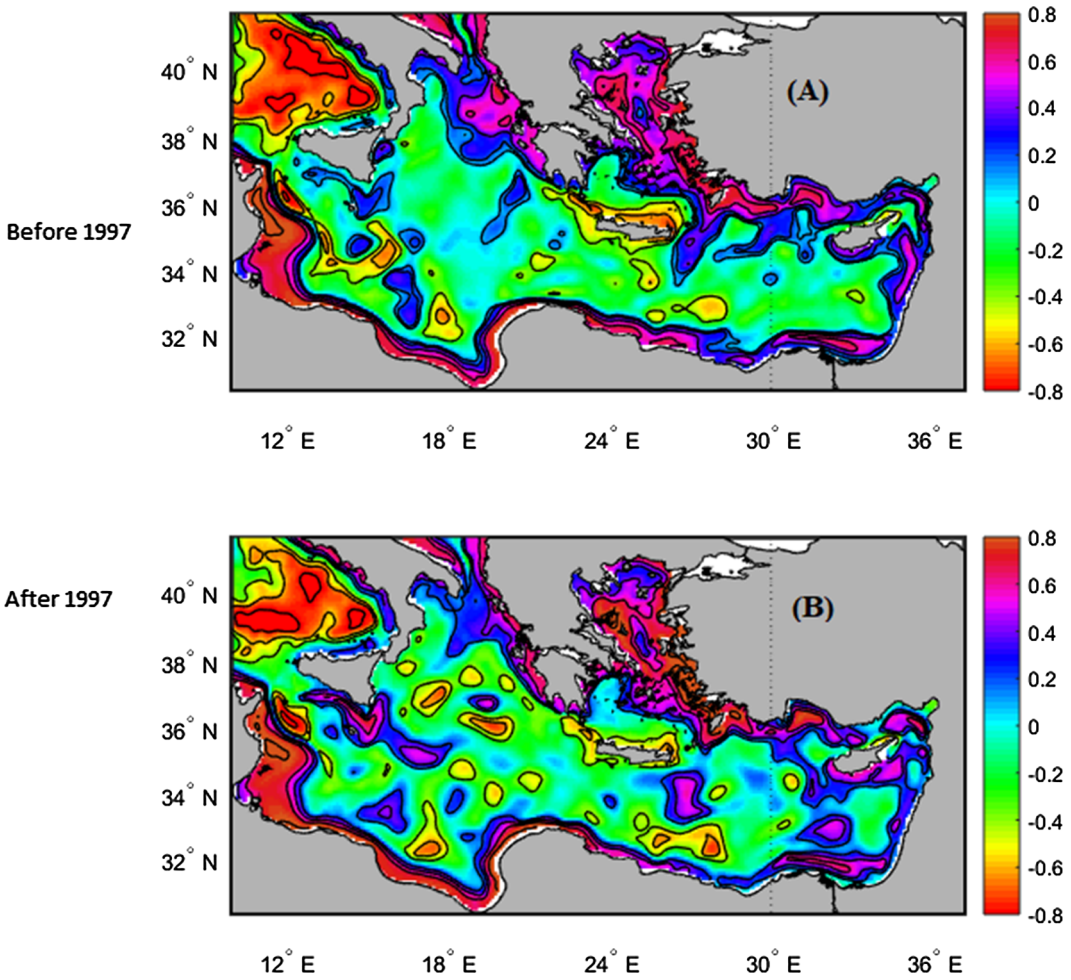

Fig. 14. Correlation pattern map between Med-ROMS SSHa averaged hindcasts (critical correlation R = 0.1 at 95% significance) and wind stress curl: (A) over the period October 1992–June 1997 and (B) over the period July 1997–December 2001.

6. Correlations between NAO index and averaged EOF-SSHa Med-ROMS hindcasts

This section discusses the correlation between NAO and averaged EOF-SSHa- Med-ROMS hindcasts to determine a linkage between the NAO index and the EMT that is responsible for north Ionian inversion. We know that the higher NAO during the 1990s is linked to the appearance of the Eastern Mediterranean Transient (Tsimplis, 2001). Fig. 17A, B and C, show the temporal evolution for NAO index with a one year moving average, Med-ROMS SSHa PC1 and PC2 for the whole simulation period 1958–2001. Note the resemblance between NAO and Med-ROMS-SSHa PC1 over the EMT period starting from 1997. Table 2 shows the correlations values between NAO index and averaged EOF-SSHa Med-ROMS hindcasts over different study periods at 95% confidence limit. We can observe a significant correlation R, at a 95% confidence limit (R = 0.41), for the period P2 between NAO one year moving average and Med-ROMS-SSHa -PC1. It is also observed that there is a statistically significant negative correlation, at 95% confidence limit, between the NAO one year moving averaged index and PC1 over the period P1 (R = −0.329) . The correlation coefficient for the whole study period revealed significant negative correlation at the same level, R = −0.284. This indicates that the large-scale climatic conditions associated with a positive NAO phase over P2 have significantly strengthened the positive correlation with the Med-SSHa PC1. On the other hand, the prevailing negative Med-ROMS- SSHa –PC1 over the period P1, as shown in Fig. 12B, is related to the negative correlation with NAO moving average index. For the Med-ROMS-SSHa PC2 we found an insignificant relationship with NAO index for the whole simulation period and P1. The multi-decadal variability in PC1 and PC2, which does not appear in NAO, might be a local Mediterranean phenomenon not related to external NAO. We also found a high significant negative correlation at a 95% confidence limit between the NAO removing averaged index and Med-ROMS-SSHa PC2 over the EMT period P2 (R = −0.488). Overall, the positive NAO indices over P2, which is considered as period of EMT, are significantly affecting the Med-ROMS-SSHa PC1 and PC2.

7. Conclusions

The results of Med-ROMS high horizontal resolution hindcasts are simulated. Each has started at the end of a previous 100-years run. The simulations have been forced with three ensemble members obtained from the corrected ERA-40 re-analyses (Pettenuzzo et al., 2010) covering the time period from January 1958 to December 2001. The model results are used to characterize the mesoscale features of the Eastern Mediterranean Sea. Both surface and subsurface eddy fields are analyzed. The circulation patterns of Med-ROMS has shown the robustness of the model in reproducing all the main general characteristics of EMED that are rich in mesoscale features. They include MMJ, AIS, AMC, Rhodes cyclonic gyre, Mersa Matruh anticyclonic gyre, western Ionian cyclonic gyre, Pelops anticyclonic gyre and Shikmona anticyclonic gyre. This is in agreement with previous studies including Robinson et al., 1991; POEM Group, 1992; Roussenov et al., 1995; Korres and Lascaratos, 2003; Pinardi et al., 2005; 2015. The monthly

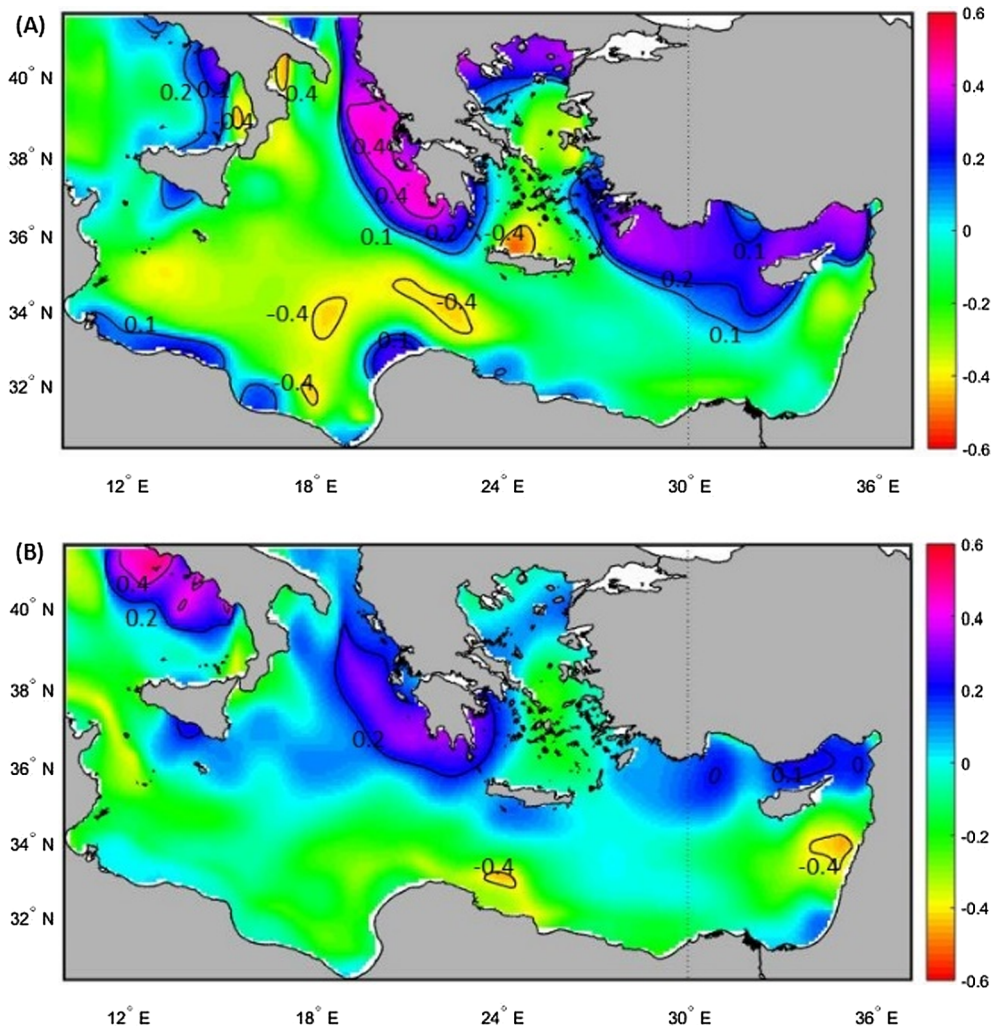

Fig. 15. Correlation pattern map between Med-ROMS-EOF1 SSHa averaged hindcasts (critical correlation R = 0.1 at 95% significance) and wind stress curl: (A) over the period October 1992–June 1997 and (B) over the period July 1997–December 2001. The solid black contour lines are for correlation coefficients 0.1, 0.2 and 0.4.

averaged near surface temperature field has suggested an intense downwelling observed at 27°E as a strong sign of Iera-Petra anticyclonic gyre. This may be due to Med-ROMS hindcast simulations being provided with corrected momentum and surface fluxes obtained from ERA-40 corrected ensembles.

The difference maps between monthly averaged Med-ROMS Hindcasts (1, 2, 3) over the simulation period January 1958–December 2001 and monthly averaged for the whole period of spin up and control run (100 years) for the salinity, velocity components and temperature are provided. The salinity difference between the two simulations was a maximum of (0.47) in front of the Libyan Coast and inside Gulf of Syrt. This can be attributed to the poor data coverage along the Libyan Coast. The basin averaged RMSE between the two simulations was only 0.106 PSU. While the maximum velocity components differences between the two simulations were about ± 0.15 m/s. The RMSE basin temperature average for the two simulations was 0.1505 °C.

There is a clear and significant resemblance in the spatial structure between the EOF1-Med-ROMS Hind 1, 2 and 3 and the EOF1 of satellite SSHa for the period October 1992 to December 2001. EOF1-SSHa for Med-ROMS hindcasts and satellite data, corresponding to a dipole. Which associated with the large negative values of SSHa (cooling) off the northern Ionian Sea and the large positive (warming) off middle and east of the Levantine Basin. While EOF2-SSHa for both Med-ROMS and satellite have a dipole located in the Ionian Sea with maximum off south Ionian Sea and minimum off north Ionian Sea. The correlation coefficients between Med-ROMS PC1 SSHa Hind 1, 2, 3 and satellite data were 0.985, 0.97 and 0.98 respectively and all values are significant at a 95% confidence limit. We have observed a strong positive signal during the 1997–1998 period from PC1 and PC2 for both Med-ROMS and Satellite SSHa. We have attributed this strong signal as associated with the relaxation of the Eastern Mediterranean Transient (EMT), producing dramatic changes in the basin-wide circulation patterns in agreement with Malanotte-Rizzoli, 2003; Skliris et al., 2007; Vervatis et al., 2013).

We have defined the Bimodal Oscillating System mechanism, responsible for decadal reversals of the Ionian basin-wide circulation (BiOS) (Gacic et al., 2011, 2014), as a pattern of climate change. Therefore, the study compared the simulated Med-ROMS hindcasts SSH with AVISO Satellite SSH. The changes associated with the 1997–1998 North Ionian reversal have been computed as a comparison between the period before the shift (P1, October 1992 – June 1997), and a period after the shift (P2, July 1997 – December 2001). The AVISO satellite SSH data availability started in October 1992. There was a similarity between Med-ROMS SSH and AVISO SSH over the period P1 in terms of the circulation pattern in the north Ionian Sea. The anticyclonic motion pattern was well presented in both Med-ROMS model and AVISO Satellite SSH but much stronger in Med-ROMS averaged hindcasts. The root mean square error RMSE difference between the Med-ROMS SSH and AVISO satellite SSH was approximately 0.0812 m. Over the period P2, the Med-ROMS successfully simulated the north Ionian inversion

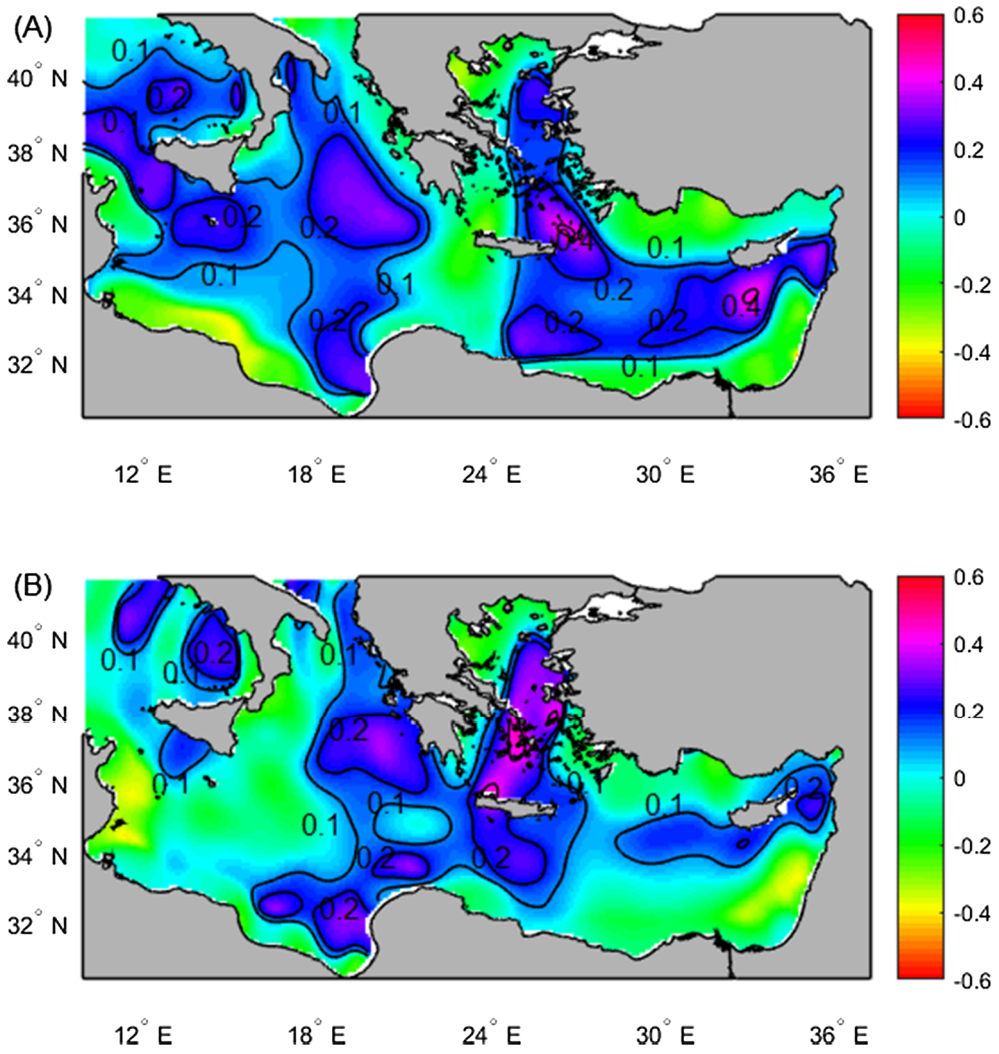

Fig. 16. Correlation pattern map between Med-ROMS-EOF2 SSHa averaged hindcasts (critical correlation R = 0.1 at 95% significance) and wind stress curl. (A) over the period October 1992–June 1997 and (B) over the period July 1997–December 2001. The solid black contour lines are for correlation coefficients 0.1, 0.2 and 0.4.

seen in the Satellite SSH, with an averaged RMSE 0.0792 m. These results highlight the robustness of Med-ROMS SSH that may be due to the improved Med-ROMS surface boundary conditions with respect to the correction added to ERA-40 Re-analysis data (Pettenuzzo et al., 2010). The wind stress curl patterns over P1 and P2 have suggested prevalent cyclonic motion in the north-eastern Mediterranean areas, while an anticyclonic motion in the southern areas of the Mediterranean Sea is in agreement with Korres et al. (2000). The wind stress map patterns have observed a slightly higher wind vorticity in the North Ionian region over P2 than the P1 period. This could be a reason for the cyclonic motion in north Ionian region, present over the whole period of P2, in agreement with Shabrang et al. (2016). This study has shown high significant correlations between the wind vorticity and Med-ROMS averaged SSHa Hindcasts over the period P1 and P2. The highest significant correlation coefficient for both periods was around 0.8 and located off the western Turkish coast inside the Aegean Sea, beside Rhodes Island. The strong significant positive correlations reflect the cyclonic motion of Rhodes Gyre. Another high positive correlation area was found along the Tunisian Coast in the Ionian. The wind stress curl was significantly correlated with the Med-ROMS SSHa averaged hindcasts with a correlation coefficient of approximately 0.6 over P1 at the North Ionian Sea. This significant correlation has dropped over P2 to be about 0.3. This could be an explanation for motion inversion over P2. We have observed a strong negative correlation of about −0.8 over the Tyrrhenian Sea in both periods. Small high positive correlations regions have appeared in the Levantine Sea. This positive correlation could be a sign for possible cyclonic motion in this regions over P2. We have computed the correlation between the wind vorticity and Med-ROMS averaged EOF-SSHa Hindcasts over the period P1 and P2. The highest correlation coefficient was approximately 0.51 along the western coast of Greece in the north east Ionian Sea. The EOF1 along the northern parts of the eastern Mediterranean Sea were significantly correlated with the wind stress curl over the period P1, except off the south-eastern Italian coast and central parts of the Aegean Sea. It was clear that in the North Ionian Sea area over the period P2, the wind stress curl was significantly correlated with the EOF1 Med-ROMS SSHa averaged hindcasts. This is confirmed by the Med-ROMS cyclonic motion in the north Ionian Sea over the same period. A highly significant negative correlation over P2 off the Israeli coast about (−0.45) between the wind vorticity and Med-ROMS averaged EOF1 SSHa Hindcasts was identified. This may be an indication of the circulation inversion first described by Pinardi and Navarra (1993). We determined positive significant correlation coefficients at a 95% confidence limit over the Eastern Mediterranean Transient period (P2) between NAO indices 12 months moving average and Med-ROMS-SSHa -PC1, while for PC2 during the same period a highly significant negative correlation at the same limit was found, R = −0.488. Therefore, our study for the Eastern Mediterranean presents evidence that the NAO and consequently wind stress curl are responsible for the North Ionian inversion. The multi-decadal variability in PC1 and PC2, which has not appeared

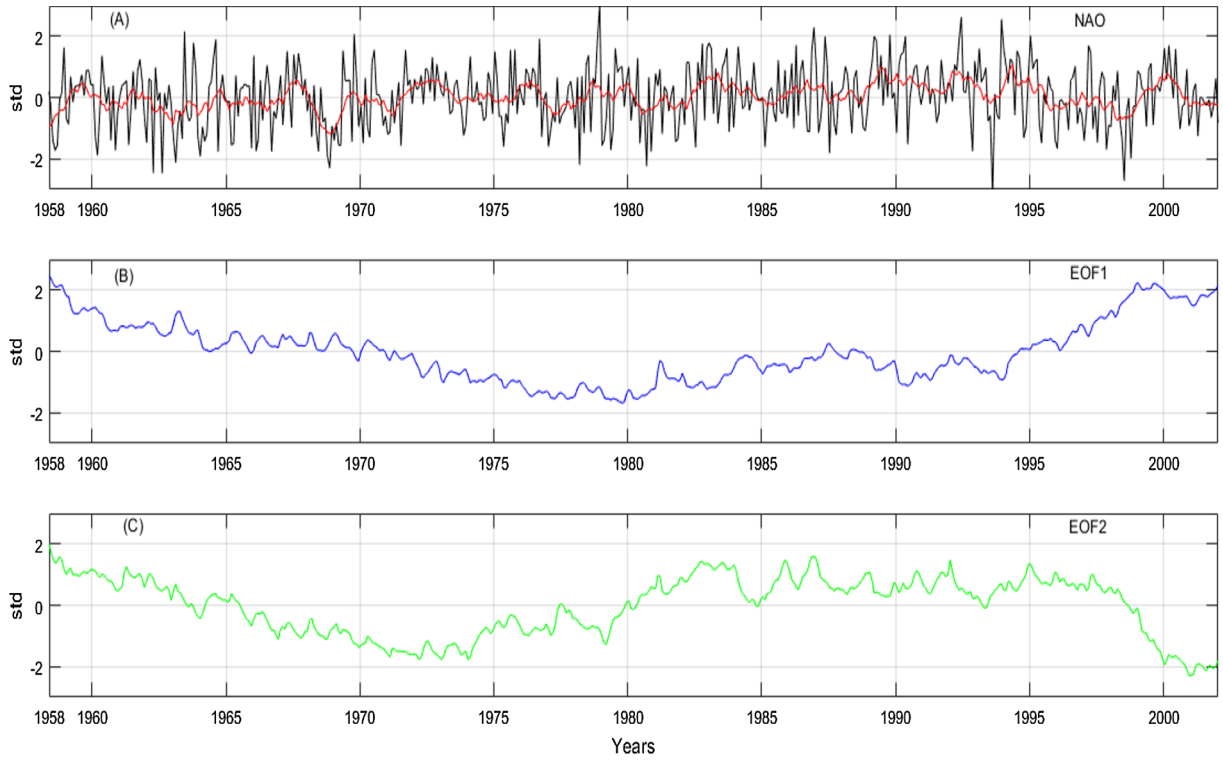

Fig. 17. Temporal evolution of the basin averaged values of: (A) The NAO index (in black) plotted in standard deviation units with their 1 year moving mean time series (red), (B) Med-ROMS-PC1-SSHa Hindcasts and (C) Med-ROMS-PC1-SSHa Hindcasts. (For interpretation of the references to colour in this figure legend, the reader is referred to the web version of this article.)

Table 2
Correlations between NAO index and averaged EOF-SSHa Med-ROMS hindcasts over different study periods at 95% confidence limit.

Time Period	Correlations between NAO index and averaged EOF-SSHa Med-ROMS hindcasts over different study periods at 95% confidence limit	
	PC1	PC2
P1	−0.329	0.018 * (Non-significant)
P2	0.41	−0.488
P1 + P2	−0.284	−0.083 * (Non-significant)

in NAO, might be a local Mediterranean phenomenon not related to external NAO.

Considerable effort is still required from the Mediterranean scientific community to further understand the driving mechanisms of the BiOS. Future work requires the use of high frequency interactive surface fluxes in order to simulate other decadal reversals systems in Mediterranean regions. In addition, inputs such as the Nile River, Suez Canal, and Marmara Sea, should be included.

Acknowledgements

We are grateful to FULBRIGHT Commission in Egypt for supporting this study. We wish to thank Prof. Nadia Pinardi and team for offering MFS products and ERA-40 corrected ensembles. Special thanks for Dr. Vincent Combes for his help in MATLAB codes. Special thank for the anonymous reviewers for helpful comments on the manuscript. Finally, I would like to express my sincere gratitude to my colleagues Dr. Eleanor ORourke and Paul Gaughan from Marine Institute in Ireland, for their wonderful collaboration in editing our manuscript.

References

Adani, M., Pinardi, N., Dobricic, S., 2011. Quality assessment of a 1985–2007 mediterranean sea reanalysis. J. Atmosph. Ocean. Technol. 569–589. https://doi.org/10.1175/2010JTECHO798.1.
Barnston, A.G., Livezey, R.E., 1987. Classification, seasonality and persistence of low frequency atmospheric circulation patterns. Mon. Weather Rev. 115, 1083–1126.
Beranger, K., Mortier, L., Gasparini, G.P., Gervasio, L., Astraldi, M., Crepon, M., 2004. The dynamics of the Sicily Strait: a comprehensive study from observations and model. Deep Sea Res. II 51, 411–440.
Berliner, L.M., Kim, Y., 2007. Bayesian design and analysis for super ensemble based climate forecasting. J. Clim. 21, 1891–1910. https://doi.org/10.1175/2007JCLI1619.1.
Beron-Vera, F.J., Ochoa, J., Ripa, P., 1999. A note on the boundary conditions for salt and freshwater balances. J. Ocean Modell. 1, 111–118.
Bjornsson, H., Venegas, A.S., 1997. A Manual for EOF and SVD Analyses of Climate Data. CCGCR Report No. 97–1. McGill University, Montréal, Québec.
Borzelli, G.L.E., Gacic, M., Cardin, V., Civitarese, G., 2009. Eastern Mediterranean transient and reversal of the Ionian Sea circulation. Geophys. Res. Lett. 36, L15108. https://doi.org/10.1029/2009GL039261.
Burnett, W.H., Price, J.A., La Violette, P.E., 1991. The surface circulation around Crete Inferred from drifter buoy trajectories and satellite imagery. Mar. Technol. Soc. Conf. 869–875.
Carniel, S., Bonaldo, D., Benetazzo, A., Bergamasco, A., Boldrin, A., Falcieri, F.M., Sclavo, M., Trincardi, F., Falcieri, F.M., Langone, L., Sclavo, M., 2016. Off-shelf fluxes across the Southern Adriatic Margin: factors controlling DenseWater-driven transport phenomena. Mar. Geol. 375, 44–63. https://doi.org/10.1016/j.margeo.2015.08.016.
Chhak, K., Di Lorenzo, E., 2007. Decadal variations in the California Current upwelling cells. Geophys. Res. Lett. 34 (L14604).
Civitarese, G., Gacic, M., Borzelli, G.L., Lipizer, M., 2010. On the impact of the Bimodal Oscillating System (BiOS) on the biogeochemistry and biology of the Adriatic and Ionian Seas (Eastern Mediterranean). Biogeosciences 7, 3987–3997.
Crisciani, F., Mosetti, R., 2016. Is the bimodal oscillating Adriatic-Ionian circulation a stochastic resonance? BGTA 57, 275–285.
Powell, T.M., Rivere, P., 2007. North Pacific Gyre Oscillation links ocean climate and ecosystem change. Geophys. Res. Lett. https://doi.org/10.1029/2007GL032838.
Demirov, E., Pinardi, N., 2002. Simulation of the Mediterranean circulation from 1979 to 1993 model simulations: Part II. Energetics of variability. J. Mar. Syst. 23–50.
Dobricic, S., Pinardi, N., Adani, M., Tonani, M., Fratianni, C., Bonazzi, A., Fernandez, V., 2007. Daily oceanographic analyses by Mediterranean Forecasting System at the basin scale. Ocean Sci. 3, 149–157.
Ducet, N., Le Traon, P.Y., Reverdin, G., 2000. Global high-resolution mapping of ocean circulation from TOPEX/Poseidon and ERS-1 and -2. J. Geophys. Res. 105,

19477–19498. https://doi.org/10.1029/2000JC900063.
El-Gindy, A., Sharaf El-Din, A.H., 1985. Water masses and circulation patterns in the deep layer of the Eastern Mediterranean. IAMP/IAPSO joint assembly, August 5-16, 1985, Honolulu, Hawai. Oceanologica Acta 9 (3) 1986.
Flather, J., 1976. A tidal model of the Northwest European Continental Shelf. Mem. Soc. R. Sci. Liege Ser. 6 (10), 141–164.
Fukumori, I.T., Cheng, Lee B., Menemenlis, D., 2004. The region pathway and destination of Nino-3 water estimated by a simulated passive tracer and its adjoint. **J.** Phys. Oceangr. 34, 582–604.
Gacic, M., Civitarese, G., Eusebi Borzelli, G.L., Kovacevic, V., Poulain, P.-M., Theocharis, A., Menna, M., Catucci, A., Zarokanellos, N., 2011. On the relationship between the decadal oscil-lations of the Northern Ionian Sea and the salinity distributions in the Eastern Mediterranean. J. Geophys. Res. 116, C12002. https://doi.org/10.1029/2011JC007280.
Gacic, M., Civitarese, G., Kovacevic, V., Ursella, L., Bensi, M., Menna, M., Cardin, V., Poulain, P.-M., Cosoli, S., Notarstefano, G., Pizzi, C., 2014. Extreme winter 2012 in the Adriatic: an example of climatic effect on the BiOS rhythm. Ocean Sci. 10, 513–522. https://doi.org/10.5194/os-10-513-2014.
Gertman, I.F., Pinardi, N., Popov, Y., Hecht, A., 2006. Aegean Sea water masses during the early stages of the Eastern Mediterranean Climatic Transient (1988–1990). J. Phys. Oceanogr. 36, 1841–1859. https://doi.org/10.1175/JPO2940.1.
Haney, R.L., 1991. On the pressure gradient force over steep bathymetry in sigma coordinates ocean models. J. Phys. Oceanogr. 21, 610–619.
Hellerman, S., Rosenstein, M., 1983. Normal monthly wind stress over the world ocean with error estimates. Phys. Oceanogr. 13, 1093–1104.
Horton, C., Kerling, J., Athey, G., Schmitz, J., Clifford, M., 1994. Airborne expendable bathy-thermograph surveys of the Eastern Mediterranean. J. Geophys. Res 99 (C5), 9891–9905.
Korres, G., Pinardi, N., Lascaratos, A., 2000. The ocean response to low frequency interannual atmospheric variability in the Mediterranean Sea. Part I. Sensitivity experiments and energy analysis. J. Clim. 13 (4), 705–731.
Korres, G., Lascaratos, A., 2003. A one-way nested eddy resolving model of the Aegean and Levantine Basins: implementation and climatological runs. J. Annales Geophysicae. 21, 205–220.
Lascaratos, A., Tsantilas, S., 1997. Study of the seasonal circle of the Ieraperta Gyre, using satellite Imager. J. Proc. Hell. Symp. Oceanogr. Fish. 1, 165–168.
Lascaratos, A., Nittis, K., 1998. A high-resolution three-dimensional numerical study of intermediate water formation in the Levantine Sea. J. Geophys. Res. 103 (C9), 18497–18511. https://doi.org/10.1029/98JC01196.
Le Traon, P.Y., Dibarboure, G., 1999. Mesoscale mapping capabilities of multi-satellite altimeter missions. J. Atmos. Oceanic Technol. 16, 1208–1223. https://doi.org/10.1175/1520-0426(1999) 016<1208:MMCOMS>2.0.CO;2.
Madec, G., Delecluse, P., Imbard, M., Levy, C., 1998. OPA 8.1 Ocean´ General Circulation Model Reference Manual, Note n. 11, Laboratoire d'Oceanographie Dynamique et de Climatologie, Institut´ Pierre Simon Laplace, Paris, France, 91 pp.
Malanotte-Rizzoli, P., 2003. Introduction to special section: physical and biochemical evolution of the eastern Mediterranean in the 1990s (PBE). J. Geophys. Res. 108 (C9), 8100. https://doi.org/10.1029/2003JC002063.
Marchesiello, P., McWilliams, J.C., Shchepetkin, A., 2001. Open boundary conditions for long term integration of regional oceanic models. J. Ocean Model. 3, 1–20.
Mihanović, H., Vilibić, I., Dunić, N., Šepić, J., 2015. Mapping of decadal middle Adriatic oceanographic variability and its relation to the BiOS regime. J. Geophys. Res. Oceans 120. https://doi.org/10.1002/2015JC010725.
Milliff, R.F., Bonazzi, A., Wikle, C.K., Pinardi, N., Berliner, L.M., 2011. Ocean ensemble forecasting. Part I: ensemble Mediterranean winds from a Bayesian hierarchical model Q. J. R. Meteorol. Soc. 137, 858–878. https://doi.org/10.1002/qj.767.
Nagy, H., Elgindy, A., Pinardi, N., Zavatarelli, M., Oddo, P., 2017. A nested pre-operational model for the Egyptian shelf zone: model configuration and validation/calibration. J. Dynam. Atmosph. Oceans 80, 75–96. https://doi.org/10.1016/j.dynatmoce.2017.10.003.
Oddo, P., Pinardi, N., 2008. Lateral open boundary conditions for nested limited area models: a process selective approach. J. Ocean Modell. 20 (2), 134–156. https://doi.org/10.1016/j.ocemod.2007.08.001.
Pettenuzzo, D., Large, W.G., Pinardi, N., 2010. On the corrections of ERA-40 surface flux products consistent with the Mediterranean heat and water budgets and the connection between basin surface total heat flux and NAO. J. Geophys. Res. 115. https://doi.org/10.1029/ 2009JC005631.
Pinardi, N., Navarra, A., 1993. Baroclinic wind adjustment processes in the Mediterranean Sea. Deep Sea Res. Part II 40, 1299–1326.
Pinardi, N., Korres, G., Lascaratos, A., Roussenov, V., Stanev, E., 1997. Numerical simulation of the interannual variability of the Mediterranean Sea upper ocean circulation. Geophys. Res. Lett. 244, 425–428.
Pinardi, N., Masetti, E., 2000. Variability of the large-scale General Circulation of the Mediterranean Sea from observation and modelling: a review. Paleogeograp. Paleoclimatol. Paleoecol. 158, 153–173.
Pinardi, N., Allen, I., Demirov, E., De Mey, P., Korres, G., Lascratos, A., Le Traon, P.Y., Maillard, C., Manzella, G., Tziavos, C., 2003. Mediterranean forecasting system: first phase of implementation (1998–2001). J. Annal. Geophys. 21, 1–21.
Pinardi, N., Arneri, E., Crise, A., Ravaioli, M., Zavatarelli, M., ., 2005. The physical, sedimentary and ecological structure and variability of shelf areas in the Mediterranean Sea. The Sea. Harvard University Chapter 32.
Pinardi, N., Coppini, G., 2010. Operational oceanography in the Mediterranean Sea: the second stage of development. Ocean Sci. 6, 263–267.
Pinardi, N., Zavatarelli, M., Adani, M., Coppini, G., Fratianni, C., Oddo, P., Simoncelli, S., Tonani, M., Lyubartsev, V., Dobricic, S., Bonaduce, A., 2015. The Mediterranean Sea large scale low frequency ocean variability from 1987 to 2007: a retrospective analysis. Prog. Oceanogr. https://doi.org/10.1016/j.pocean.2013.11.003.
POEM Group, 1992. General circulation of the Eastern Mediterranean. Earth Sci. Rev. 32, 285–309.
Preisendorfer, R. W., 1988. Principal component analysis in meteorology and oceanography. Amsterdam.
Pujol, M.-I., Larnicol, G., 2005. Mediterranean Sea eddy kinetic energy variability from 11 years of altimetric data. J. Mar. Syst. 58 (3–4), 121–142. https://doi.org/10.1016/j.jmarsys.2005.07.005.
Rio, M.-H., Poulain, P.-M., Pascual, A., Mauri, E., Larnico, G., 2005. Mediterranean Sea eddy kinetic energy variability from 11 years of altimetric data. J. Mar. Syst. 58 (3), 121–142.
Robinson, A.R., Golnaraghi, M., Lesilie, W.G., Artigiani, A., Hecht, A., Lazzoni, E., Michelato, A., Sansone, E., Theocharis, A., Unluta, U., 1991. The Eastern Mediterranean general circulation: features structure and variability. J. Dynam. Atmosph. Ocean. 15, 215–240.
Roether, W., Manca, B.B., Klein, B., Bregant, D., Georgopoulos, D., Beitzel, V., Kovacevic, V., Luchetta, A., 1996. Recent changes in the eastern Mediterranean deep waters. Science 271, 333–335.
Roussenov, V., Stanev, E., Artale, V., Pinardi, N., 1995. A seasonal model of the Mediterranean Sea general circulation. J. Geophys. Res. 100, 13515–13538.
Sanchez-Gomez, E., Somot, S., Josey, S.A., Dubois, C., Elguindi, N., Déqué, M., 2011. Evaluation of the Mediterranean Sea water and heat budgets as simulated by an ensemble of high resolution regional climate models. Clim. Dyn. 37, 2067–2086.
Shabrang, L., Menna, M., Pizzi, C., Lavigne, H., Civitarese, G., Gacic, M., 2016. Long-term variability of the southern Adriatic circulation in relation to North Atlantic Oscillation. Ocean Sci. 12, 233–241. https://doi.org/10.5194/os-12-233-2016.
Shchepetkin, A.F., McWilliams, J.C., 2005. The regional oceanic modelling system (ROMS): a split-explicit, free-surface, topography following coordinate oceanic model. Ocean Modell. 9, 347–404. https://doi.org/10.1016/j.ocemod.2004.08.002.
Skliris, N., Sofianos, S., Lascaratos, A., 2007. Hydrological changes in the Mediterranean Sea in relation to changes in the freshwater budget: a numerical modelling study. J. Mar. Syst. 65, 400–416.
Theocharis, A., Balopoulos, E., Kioroglou, S., Kontoyiannis, H., Iona, A., 1999. A synthesis of the circulation and hydrography of the South Aegean Sea and the Straits of the Cretan Arc (March 1994- January 1995). J. Prog. Oceanogr.. 44, 469–509.
Tsimplis, M.N., 2001. Forcing of the Mediterranean Sea by atmospheric oscillations over the North Atlantic. Geophys. Res. Lett. 28 (5), 803–806.
Tonani, M., Pinardi, N., Dobricic, S., Pujol, I., Fratianni, C., 2008. A high-resolution free-surface model of the Mediterranean Sea. Ocean Sci. 4, 1–14.
Uppala, S.M., Kållberg, P.W., Simmons, A.J., Andrae, U., da Costa Bechtold, V., Fiorino, M., Gibson, J.K., Haseler, J., Hernandez, A., Kelly, G.A., Li, X., Onogi, K., Saarinen, S., Sokka, N., Allan, R.P., Andersson, E., Arpe, K., Balmaseda, M.A., Beljaars, A.C.M., van de Berg, L., Bidlot, J., Bormann, N., Caires, S., Chevallier, F., Dethof, A., Dragosavac, M., Fisher, M., Fuentes, M., Hagemann, S., Hólm, E., Hoskins, B.J., Isaksen, L., Janssen, P.A.E.M., Jenne, R., McNally, A.P., Mahfouf, J.-F., Morcrette, J.-J., Rayner, N.A., Saunders, R.W., Simon, P., Sterl, A., Trenberth, K.E., Untch, A., Vasiljevic, D., Viterbo, P., Woollen, J., 2005. The ERA-40 re-analysis. Q. J. R. Meteorol. Soc. 131, 2961–3012. https://doi.org/10.1256/qj.04.176.
Verri, G., Pinardi, N., Oddo, P., Ciliberti, S.A., Coppini, G., 2018. River runoff influences on the Central Mediterranean overturning circulation. Clim. Dyn. https://doi.org/10.1007/s00382-017-3715-9.
Vervatis, V.D., Sofanos, S.S., Skliris, N., Somot, S., Lascaratos, A., Rixen, M., 2013. Mechanisms controlling the thermohaline circulation pattern variability in the Aegean-Levantine region. A hindcast on coastal zone of simulation (1960–2000) with an eddy resolving model. Deep Sea Res. Part I Oceanogr. Res. Pap. Hist. Med. Assoc. 74, 82–97.
Vukicevic, T., Hess, P., 2000. Analysis of tropospheric transport in the Pacific Basin using the adjoint techniques. J. Geophys. Res. 105, 7213–7230.
Wu, P., Haines, K., 1998. The General Circulation of the Mediterranean Sea from a 100-year simulation. J. Geophys. Res. 103, 1121–1135.
Zavatarelli, M., Pinardi, N., Kourafalou, V.H., Maggiore, A., 2002. Diagnostic and prognostic model studies of the Adriatic Sea circulation. Seasonal variability. J. Geophys. Res. 107 Ant. No. 3004.